Role of land surface processes in monsoon development: East Asia and West Africa

Yongkang Xue,[1,2] H.-M. H. Juang,[3] W.-P. Li,[1] S. Prince,[4] R. DeFries,[4,5] Y. Jiao,[6] and R. Vasic[1]

Received 3 March 2003; revised 3 November 2003; accepted 14 November 2003; published 6 February 2004.

[1] Evidence is presented that exchanges of water and energy between the vegetation and the atmosphere play an important role in east Asian and West African monsoon development and are among the most important mechanisms governing the development of the monsoon. The results were obtained by conducting simulations for five months of 1987 using a general circulation model (GCM) coupled with two different land surface parameterizations, with and without explicit vegetation representations, referred to as the GCM/vegetation and the GCM/soil, respectively. The two land surface models produced similar results at the planetary scale but substantial differences at regional scales, especially in the monsoon regions and some of the large continental areas. In the simulation with GCM/soil, the east Asian summer monsoon moisture transport and precipitation were too strong in the premonsoon season, and an important east Asian monsoon feature, the abrupt monsoon northward jump, was unclear. In the GCM/vegetation simulation, the abrupt northward jump and other monsoon evolution processes were simulated, such as the large-scale turning of the low-level airflow during the early monsoon stage in both regions. With improved initial soil moisture and vegetation maps, the intensity and spatial distribution of the summer precipitation were also improved. The two land surface representations produced different longitudinal and latitudinal sensible heat gradients at the surface that, in turn, influenced the low-level temperature and pressure gradients, wind flow (through geostrophic balance), and moisture transport. It is suggested that the great east-west thermal gradient may contribute to the abrupt northward jump and the latitudinal heating gradient may contribute to the clockwise and counterclockwise turning of the low-level wind. The results showed that under unstable atmospheric conditions, not only low-frequency mean forcings from the land surface, such as monthly mean albedo, but also the perturbation processes of vegetation were important to the monsoon evolution, affecting its intensity, the spatial distribution of precipitation, and associated circulation at the continental scale.
INDEX TERMS: 1866 Hydrology: Soil moisture; 1833 Hydrology: Hydroclimatology; 3322 Meteorology and Atmospheric Dynamics: Land/atmosphere interactions; 3337 Meteorology and Atmospheric Dynamics: Numerical modeling and data assimilation; *KEYWORDS:* land surface, monsoon, SSiB

Citation: Xue, Y., H.-M. H. Juang, W.-P. Li, S. Prince, R. DeFries, Y. Jiao, and R. Vasic (2004), Role of land surface processes in monsoon development: East Asia and West Africa, *J. Geophys. Res.*, *109*, D03105, doi:10.1029/2003JD003556.

1. Introduction

[2] Monsoons are macroscale phenomena. Differential heating of the land and the ocean, latent heat release into the atmosphere, and planetary rotation are considered to be the factors that determine the strength, duration and spatial distribution of large-scale monsoons [*Webster et al.*, 1998]. Land surface characteristics of the continents have also been suggested to be an important factor in the modulation of the monsoon circulation and surface hydrology [*Webster*, 1987]. Despite the importance of the monsoon systems in providing water for agriculture in some of the Earth's most populous regions monsoons have not been adequately modeled (see *Webster et al.* [1998] for a comprehensive review) and the role of land surface processes in the systems are still not well understood.

[1]Department of Geography, University of California, Los Angeles, California, USA.
[2]Department of Atmospheric Sciences, University of California, Los Angeles, California, USA.
[3]National Centers for Environmental Prediction, National Oceanic and Atmospheric Administration, Camp Springs, Maryland, USA.
[4]Department of Geography, University of Maryland, College Park, Maryland, USA.
[5]Earth System Science Interdisciplinary Center, University of Maryland, College Park, Maryland, USA.
[6]Department of Earth and Atmospheric Sciences, University of Quebec at Montreal, Montreal, Canada.

0148-0227/04/2003JD003556$09.00

[3] In the case of the Indian monsoon, for example, the role of Eurasian snow cover is not agreed. Although many observational studies [e.g., *Hahn and Shukla*, 1976; *Dey and Bhanu Kumar*, 1982; *Liu and Yanai*, 2002] generally show a negative correlation between Eurasian snow cover and subsequent summer Indian monsoon, modeling studies with general circulation models of the atmosphere (GCM) and regional models [e.g., *Barnett et al.*, 1989; *Yasunari et al.*, 1991; *Vernekar et al.*, 1995; *Douville and Royer*, 1996] indicate that the effects of anomalous snow cover over Eurasia on the Indian monsoon are highly variable (see *Douville and Royer* [1996] for a review). A recent study using observational data has challenged this relationship [*Robock et al.*, 2003].

[4] In addition to snow, a number of studies have explored the roles of other land surface processes and the mechanisms that govern land surface/monsoon interactions in monsoon systems. In an investigation of the relative roles of land surface evaporation and sea surface temperature (SST) on the Asian monsoon [*Lau and Bua*, 1998], it was found that land/atmosphere interactions did not seem to alter basic, planetary-scale features, but local effects over east Asia/Indochina were quite pronounced. In a sensitivity study, *Meehl* [1994] found that stronger Asian summer monsoon were associated with lower surface albedo, greater soil moisture, less snow cover, and greater sea/land contrast. *Douville et al.* [2001] indicated that although African summer rainfall increased with increased soil moisture, there was no response in the Indian subcontinent, which they attributed to the more dynamic and chaotic nature of the Asian monsoon. A GCM simulation of the desertification in Mongolian and Inner Mongolian grassland [*Xue*, 1996] produced negative monsoon rainfall anomalies in northern and southern China and positive rainfall anomalies along the Changjiang (Yangtze) river region, which were generally consistent with observed anomalies. The large reduction in evaporation due to land degradation resulted in less convection and lowered atmospheric heating rates, which was associated with relative subsidence and, in turn, weakened the northward movement of the monsoon flow and lowered the rainfall and evaporation, leading to a positive feedback system.

[5] In this study, we used the National Center for Environmental Prediction's (NCEP) GCM which belongs in the higher hierarchy of numerical models used for climate studies [*Kalnay et al.*, 1990; *Kanamitsu et al.*, 1991]. The Simplified Simple Biosphere model (SSiB) [*Xue et al.*, 1991] was coupled with the NCEP GCM for this study. The simulations with the NCEP GCM/SSiB were compared with those from the NCEP GCM coupled with a land scheme where the biophysical processes were not explicitly parameterized. Using these comparisons, we explored the influence of the soil and vegetation biophysical processes on intraseasonal monsoon development. This study focuses mainly on the impact of land surface processes on monsoon precipitation. This paper discusses the monsoons in east Asia and West Africa; in another paper we will focus on the Americas.

2. Model Descriptions

[6] The NCEP GCM (*Kalnay et al.* [1990], *Kanamitsu et al.* [1991], http://sgi62.wwb.noaa.gov:8080/research/mrf.html) was used with 28 levels and with T62 horizontal resolution (slightly less than 2 degrees in equatorial and midlatitude areas) for a range of model runs. The effects of using the GCM coupled with a simple two-layer soil model (NCEP GCM/SOIL), as used in the original NCEP GCM, were compared with the GCM coupled with SSiB [*Xue et al.*, 1991] (NCEP GCM/SSiB), a comprehensive soil-vegetation-atmosphere model. The two land parameterization schemes represent land surface processes with two different approaches.

[7] In NCEP GCM/SOIL the ground hydrology was simulated by the soil model, and the distributions of monthly mean vegetation albedo and surface roughness length were separately prescribed on the basis of an existing data set [*Dorman and Sellers*, 1989], which has similar monthly mean values to those used in SSiB, but no explicit biophysical processes are included. Soil temperature and soil volumetric water content were computed in two layers at depths 0.1 and 1.0 m in a fully implicit time integration scheme [*Pan and Mahrt*, 1987]. The lowest atmospheric model layer was the surface layer and the Monin-Obukhov similarity profile relationship was applied to obtain the surface stress and sensible and latent heat fluxes [*Miyakoda and Sirutis*, 1986]. A bulk aerodynamic formula was used to calculate the fluxes once the turbulent exchange coefficients had been obtained. In this approach the land surface properties that regulate land/atmosphere interactions were regarded as separable parameters, which could be independently prescribed as boundary conditions in the GCM for each month.

[8] In NCEP GCM/SSiB the radiative transfer in the canopy was simulated, which produces diurnal variation in surface albedo. There were three soil layers and one vegetation layer. *Deardorff*'s [1977] force-restore method was used to predict the surface and the deep soil temperatures. SSiB includes processes such as water interception loss, direct evaporation from bare soil, and canopy transpiration (controlled by photosynthesis), to describe the surface water balance. The aerodynamic resistance controls interactions of heat fluxes between the vegetated surface and the atmosphere. Similarity theory was used to calculate the aerodynamic resistance from the canopy to the reference height. On the basis of the *Paulson* [1970] and *Businger et al.* [1971] equations, a relationship between the Richardson number, vegetation properties, and aerodynamic resistance at the vegetated surface was developed. Many GCMs use *Louis'* [1979] parameterization to calculate the aerodynamic resistance, where the total aerodynamic resistance including both neutral and non-neutral parts is a function of the Richardson number. This implies that only one value of surface roughness length is used for the parameterization. Although this parameterization is simple and easy to use, it does not satisfy the vegetated surface, where the range of values of surface roughness length could be as large as 1 order of magnitude. In SSiB, the resistance of the neutral part is dependent on vegetation and soil properties. In the non-neutral part, a parameterization is related to atmospheric stability conditions and some adjustments based on the vegetation conditions are introduced [*Xue et al.*, 1991, 1996a].

[9] In the NCEP GCM/SSiB model, land surface properties were specified according to vegetation-cover type. A

Table 1. Designations of the Model Runs and the Different Initial and Boundary Conditions Used

Case	Model	Initial Conditions	Land Cover Map
C	NCEP/SOIL	Reanalysis	none
S1	NCEP/SSiB	Reanalysis	NEW SSiB MAP
S2	NCEP/SSiB	Reanalysis and GSWP initial soil moisture	NEW SSiB MAP
S3	NCEP/SSiB	Reanalysis	OLD SSiB MAP

parameter set for each of the vegetation types was used on the basis of a variety of sources [*Dorman and Sellers*, 1989; *Willmott and Klink*, 1986; *Xue et al.*, 1996a, 1996b], many of which are invariant with season. Seasonally varying monthly values of some vegetation properties, such as leaf area index (LAI), green leaf fraction, and surface roughness length, were prescribed for most vegetation types or calculated in the model for the crop type [*Xue et al.*, 1996b]. SSiB provided fluxes of momentum, sensible heat and latent heat, radiative skin temperature, visible and near-infrared albedo for both direct and diffuse radiative to the GCM.

3. Experimental Design and Initial and Boundary Conditions

[10] The GCM simulations consisted of five month-long integrations through the boreal monsoon season. Initial conditions were obtained from NCEP/NCAR Global Reanalysis for three dates, 1, 3, and 4 May 1987. The date 2 May was skipped because of errors in the reanalysis data for that day. 1987 was an ENSO year and was 1 of 2 years for which a comprehensive soil moisture data set was available. The results of the three model runs with different initial conditions (1, 3, and 4 May) were averaged. The NCEP GCM/SOIL and the NCEP GCM/SSiB runs are referred to as cases C and S1, respectively (Table 1).

[11] The means of surface albedo for case C and case S1 were very similar during June-July-August (JJA) with the exception of some, mostly dry, areas where SSiB simulated slightly higher values (Figure 1). The 1987 NCEP/NCAR Global Reanalysis [*Kalnay et al.*, 1996; *Kistler et al.*, 1999] (referred to as Reanalysis) was used in both case C and case S1 as the source of initial conditions (atmosphere, soil moisture, and soil temperatures), ocean surface boundary conditions (SST and sea ice), and initial snow depth for all GCM runs, as originally used by NCEP for prediction/forecasting. Comparisons between these two cases indicate the effects of explicit description of biophysical processes in the GCM.

[12] Soil moisture was simulated in both GCM/SSiB and GCM/SOIL during model simulations without nudging. Specified SST and sea ice were updated using the observational data during the simulation. Observational data for verification were from the Climate Prediction Center Merged Analysis of Precipitation (CMAP) [*Xie and Arkin*, 1997] in which observations from rain gauges were merged with precipitation estimates from satellite system.

[13] The impact of initial soil moisture on the model simulations was studied using soil moisture data from the GEWEX soil wetness project (GSWP) [*Dirmeyer et al.*, 1999]. GSWP is a pilot study intended to produce a soil wetness global data set by using 1987 and 1988 meteorological observations and analyses to drive land surface models. SSiB participated in this project and the results produced by SSiB were used for this study. The average of three runs using initial soil moisture from GSWP in the NCEP GCM/SSiB is referred to as case S2 and comparisons between cases S1 and S2 indicate the effects of the different initial soil moisture.

[14] For numerical simulations with the NCEP GCM/SSiB, a global vegetation classification map was used in the coupled surface-atmosphere model to provide land surface conditions required by the SSiB. A 1 km^2 resolution global land cover map, based on remote sensing [*Hansen et al.*, 2000] (referred to as NEW SSiB MAP) was used in cases S1 and S2. The vegetation map was aggregated to the GCM grid system by grouping the cover types into the 12 SSiB vegetation types [*Xue et al.*, 2001] and selecting the most common type in each T62 cell (Figure 2a). The land cover classes originally used in SSiB were based on the physiognomic classification of *Kuchler* [1983] and the land use database of *Matthews* [1984, 1985] (referred to as OLD SSiB MAP, Figure 2b). OLD SSiB MAP was used in case S3.

[15] The most significant differences between NEW SSiB MAP and OLD SSiB MAP were in semi-arid and arid areas (Figure 2). For example, OLD SSiB MAP classified central Asia, including the Tibetan plateau, as desert, which is not appropriate [*Shi and Smith*, 1992], while in NEW SSiB MAP it was classified as grasslands or shrubs with bare soil. OLD SSiB MAP classified the Sahara desert as bare soil and shrubs with bare soil; NEW SSiB MAP classified it as bare soil only. In addition to central Asia and the Sahara desert, in NEW SSiB MAP, Europe had more cropped area and India's vegetation cover was changed from crops and forests to wooded grassland and small areas of grassland and shrubs. The comparison between cases S1 and S3 allowed comparison of the effects of the land cover maps.

4. Simulation Results

4.1. General Features

[16] The JJA period is the monsoon season for many areas in the Northern Hemisphere. Case C simulated the spatial distribution of JJA precipitation reasonably (Figure 3) with the maximum values in the Inter-Tropical Convergence Zone (ITCZ) and a second peak in the midlatitudes of both hemispheres. The monsoon regions in India, east Asia, Africa, and the Americas were evident. The main deficiencies in the simulation were the rather weak precipitation in the West Pacific (the Mei-Yu or "Plum" rainband of east Asia and southern Japan), too strong precipitation in the east Pacific, and excessively large area of light-precipitation at higher latitudes (Figure 3c).

[17] Case S1 produced very similar spatial distributions of precipitation as case C at the planetary scale (not shown), but there were substantial differences at regional/continental scales (Figure 3d). These were mainly in tropical and subtropical monsoon areas, and in midlatitude and high-latitude continents. For instance, case S1 increased the precipitation in Central America, reduced the precipitation in southern China and India, including oceans nearby, and increased precipitation along the Asian monsoon trough (south and east of the Tibetan Plateau). It also eliminated the excess precipitation in some continental areas and increased the precipitation in West Africa. We next inves-

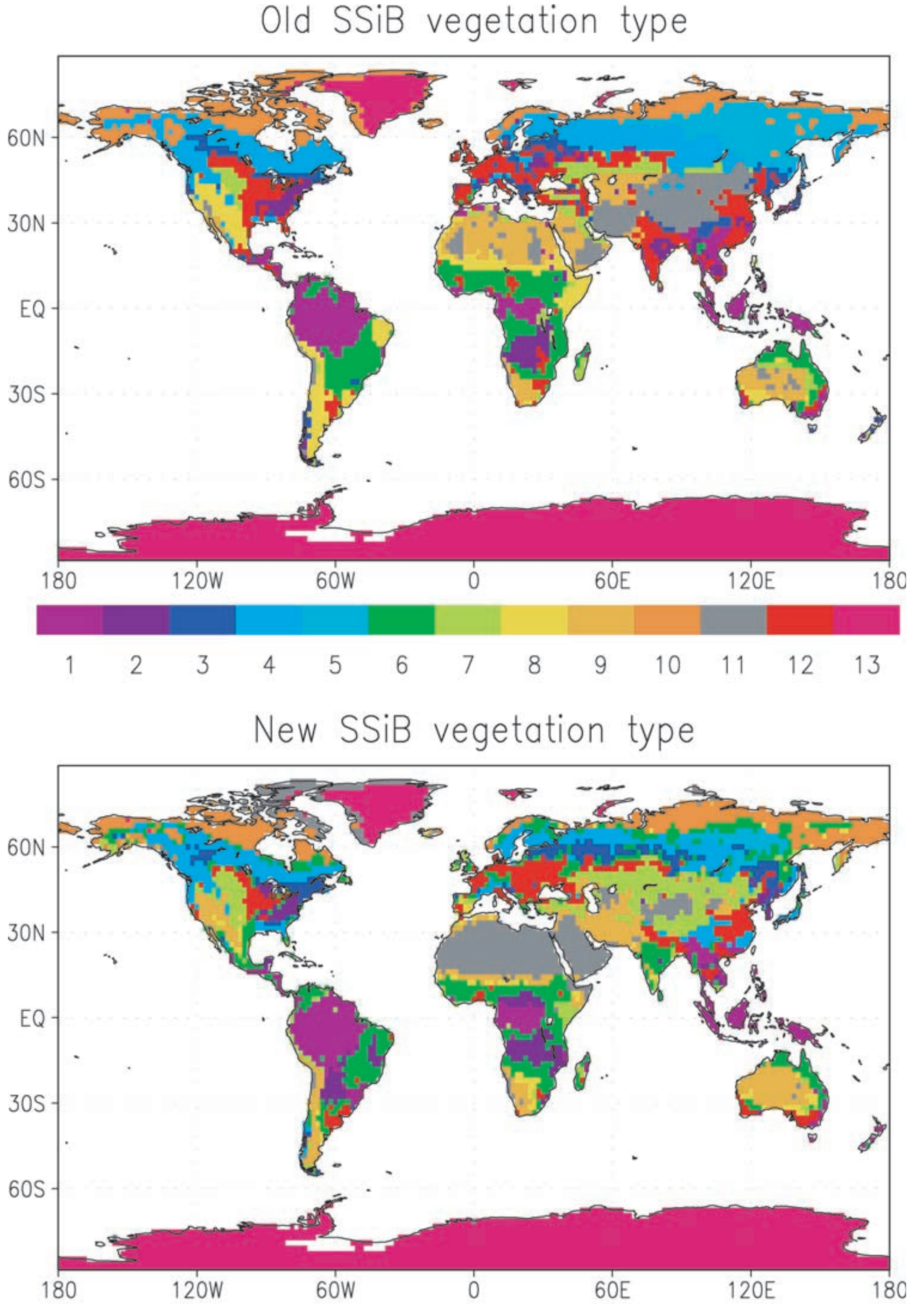

Figure 1. NCEP GCM/SSiB land cover classification map. (top) OLD SSiB MAP; (bottom) NEW SSiB MAP. Type 1, tropical rain forest; type 2, broadleaf deciduous trees; type 3, broadleaf and needleleaf trees; type 4, needleleaf evergreen trees; type 5, needleleaf deciduous trees; type 6, broadleaf trees with ground cover; type 7, grassland; type 8, broadleaf shrubs with ground cover; type 9, broadleaf shrubs with bare soil; type 10, dwarf trees with ground cover; type 11, desert; type 12, crops; type 13, permanent ice.

tigate whether these regional differences were associated with land surface processes.

4.2. East Asian Simulation

[18] The east Asian monsoon covers China, Korea, Japan, Indochina, as well as parts of surrounding countries and nearby oceans and, together with the Indian monsoon, forms the major part of the Asian Monsoon system [*Flohn*, 1957; *Ding*, 1994]. The observed precipitation over east Asia had strong seasonal, interannual, and inter-decadal variations, in particular a dramatic shift from dry condition to wet condition in central eastern China and an opposite

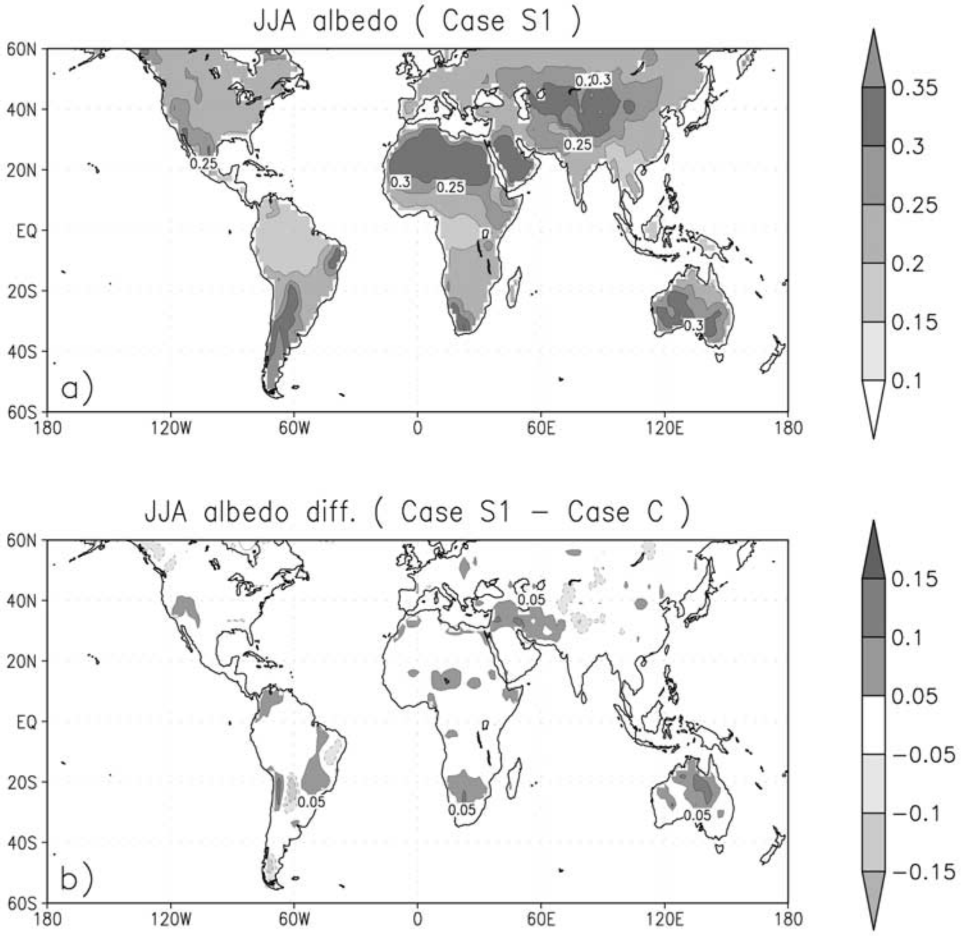

Figure 2. JJA average albedo for (a) case C; (b) case S1−case C.

shift in northern China in the 1970s [*Chen et al.*, 1991; *Ding*, 1994; *Yatagai and Yasunari*, 1994; *Yanai and Tomita*, 1998; *Weng et al.*, 1999], related to the El Niño-like SST anomalies [e.g., *Yang and Lau*, 1998; *Weng et al.*, 1999], midlatitude circulation, Indian monsoon [*Chen et al.*, 1991; *Yatagai and Yasunari*, 1995], and land surface processes such as snow and land degradation [e.g., *Yasunari et al.*, 1991; *Vernekar et al.*, 1995; *Xue*, 1996].

4.2.1. Evolution of the East Asian Monsoon

[19] The rainy season in east Asia starts from south of the Changjiang river in April and moves southward to South China in May with light precipitation. This is caused by the confluence of cold air from north and the southwesterly flow from subtropical high and westerly flow from the subtropical region of south Asia, forming a typical subtropical rain belt [*Chen et al.*, 2001]. In mid-May, the tropical monsoon develops in the South China Sea and large amounts of moisture are transported northward into the east Asian continent. Heavy precipitation occurs first in South China and moves northward, indicating a pre-Mei-Yu season. The CMAP precipitation for May 1987 (Figure 4a) indicated a precipitation center in the coastal region of South China with a northeast-southwest precipitation belt. The 4–6 mm d^{-1} isohyet was located slightly north of the Changjiang river.

[20] Case C simulated the south-north gradient of the spatial distribution of the precipitation in the pre-Mei-Yu season. The rainfall maximum was centered on the Changjiang river with a south-north precipitation belt (Figure 4b). The 4–6 mm d^{-1} isohyet extended much farther to the north, almost reaching Inner Mongolia. Compared to case C, the spatial distribution of the precipitation in case S1 was shifted to the south (Figure 4c). The 4–6 mm d^{-1} isohyet was located to the south of the Yellow River, and the center of the maximum precipitation was located to the south of the Changjiang river with a northeast-southwest precipitation belt. The observed, case C, and case S1 average precipitation over 110°E ~ 120°E and 20°N ~ 40°N was 5.96, 6.51 (±0.5), and 5.74 (±0.4) mm d^{-1}, respectively. The results for case S2 in Figure 4d will be presented in Section 5.

[21] We focused on the results from the three case means to minimize the effects of spurious results and standard deviations are given for all the results presented in the paper (in parentheses). To check the reliability of the results, we also compared the precipitation patterns in Figure 4 with those for each pair of runs in case C and case S1 and found they were very similar. In all three initial conditions, the positions of the 2–4 mm d^{-1} isohyets in case C were 5 to 10 degree to the north compared to those in case S1. The monthly mean precipitation over 110°E ~ 120°E and 30°N ~ 40°N (north of the Changjiang river) was 6.48, 5.1, and 7.08 mm d^{-1} for runs in case C and 4.15, 3.25, and 4.44 mm d^{-1} for runs in case S1, which indicated a

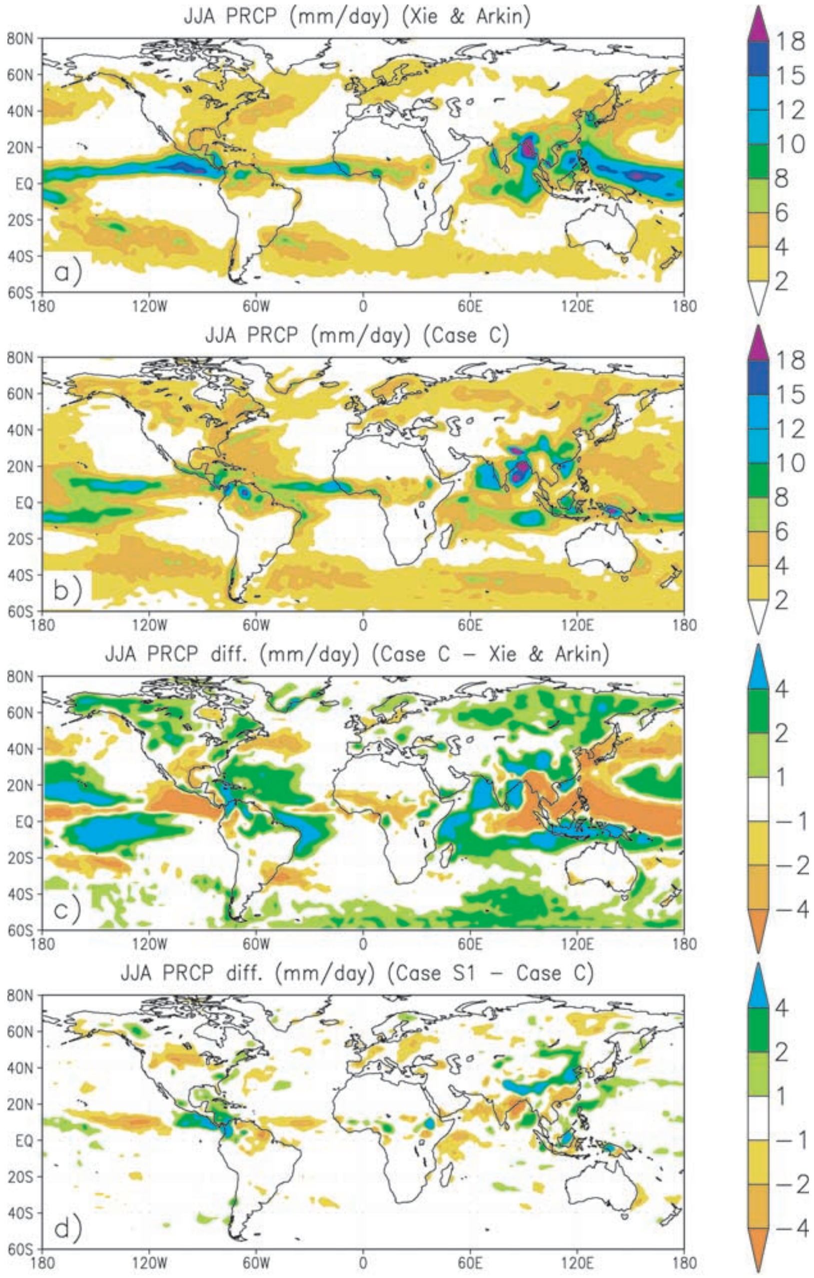

Figure 3. JJA 1987 precipitation for (a) CMAP; (b) case C; (c) case C–CMAP; (d) case S1–case C (mm d^{-1}).

consistently farther north extension of precipitation in case C. The precipitation was 2.98 mm d^{-1} for observation over that area. The highest rainfall in case S1 for this area was lower than the lowest rainfall in case C. This showed that the differences between cases S1 and C were significant.

[22] Both case C and case S1 produced spuriously heavy rainfall in a region centered at 104°E and 33°N. Because the Loess Plateau is to the north of this area and the Sichuan Basin is to the south, there is a steep topographic gradient and the complex regional topography may have contributed to this simulation error. This spurious simulation of precipitation also occurred in the NCEP Reanalysis, and fifth generation Penn State University/NCAR Meso-scale Model (PSU/NCAR MM5) [*Grell et al.*, 1994] with 50 km horizontal resolution (W. Li, personal communication, 2002).

[23] The east Asian premonsoon and monsoon evolution during the rainy season is illustrated by the zonally averaged, 10-day mean precipitation between 105°E and 120°E from May through September (Figure 5). The observed time evolution of the May–September precipitation in 1987 (Figure 5a) was similar to that of *Chen et al.* [2001, Figure 2a] and *Lau et al.* [1988, Figure 7], both of which are the means of observational data, 1961–1995 and 1950–1979, respectively.

[24] Intense precipitation originated around 27°N in early May and by late May had moved southward to about 22°N (Figure 5a, solid arrow). In June the heavy rain moved abruptly northward (dashed arrow) and another precipitation maximum appeared to the north of 30°N. This point marks the start of the Mei-Yu rains. This development is an

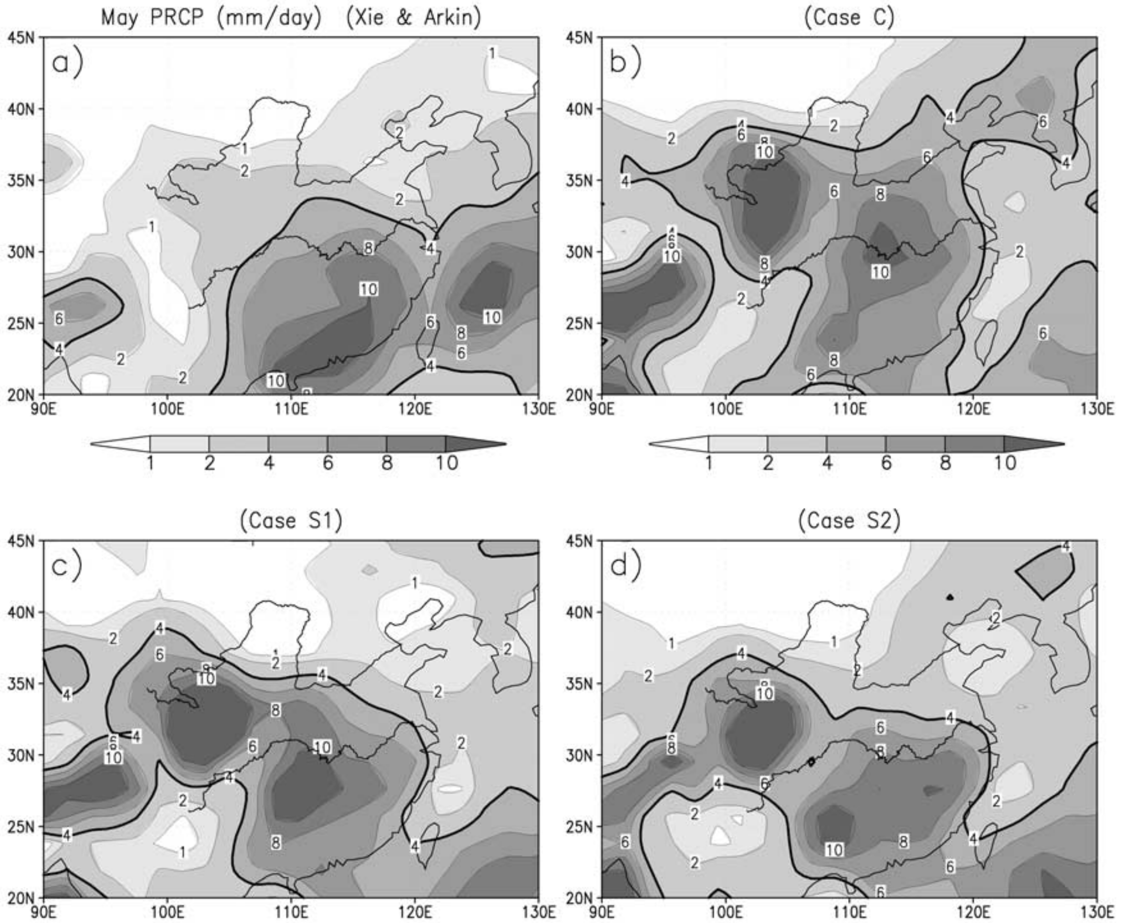

Figure 4. May 1987 precipitation for (a) CMAP; (b) case C; (c) case S1; (d) case S2 (mm d^{-1}).

important signature of the east Asian monsoon, and is referred to as the abrupt monsoon northward jump and has been described in numerous studies [e.g., *Lau et al.*, 1988; *Chen et al.*, 1991; *Ding*, 1994]. According to climatological data [e.g., *Lau et al.*, 1988], the monsoon rain expands farther into northern China (about 40°N) from July to August and initiates another jump, leading to the start of the monsoon season in northern China. In 1987, this second jump was not clear and there was only a gradual expansion of the rainfall band. There was a relatively dry area between 25°N and 30°N during part of July and August. The monsoon then retreated southward in late August and early September (solid arrow).

[25] There are clear differences between cases C and S1 simulations of the evolution of the monsoon (Figures 5b and 5c). Case C correctly simulated the rainy season, the south-north precipitation gradient, as well as the rainfall peak in July between 20°N and 25°N (Figure 5b). However, the monsoon evolution process was unclear. In addition to the overly extended precipitation in May as discussed above, there was only one persistent wet season during the entire period with the maximum precipitation located around 23°N (coast of South China). This pattern persisted in all three runs in case C. Furthermore, the simulated rain was more intense than that indicated by the observations. Case S1, on the other hand, simulated the features of the monsoon evolution and captured the northward jump. The northward jump, however, started about 10d earlier and extended over a slightly longer period (Figure 5c, dashed arrow). The rainfall maxima around 22°N and 32°N were simulated, but expanded to northern China too early. The intensity was also stronger than observed (Figure 3d). Overall, however, the evolution processes were simulated, including the dry area between 25°N and 30°N during July and August. All three runs in case S1 were consistent, but with slightly different dates for the start of the abrupt northward movement and their durations. The results for case S2 and case S3 in Figure 5 will be discussed in sections 5 and 6, respectively.

4.2.2. Physical and Dynamic Mechanisms of Land Surface and Atmospheric Effects

[26] The differences between cases C and S1 were caused only by the different parameterizations of land surface processes. These affect the water and energy balances on land surface and then the atmosphere through land/atmosphere interactions. In May, southwest airflow brought moisture to the southern part of China and formed a cyclone-like system according to Reanalysis (Figure 6a). The strong convergence zone at 850 hPa to the south of the Changjiang river was consistent with the observed precipitation. To the north of 35°N, westerly winds and divergence prevailed. The bold lines in the figure show the locations where the zonal wind was zero for a better view of the circulation patterns. Case C produced a convergence

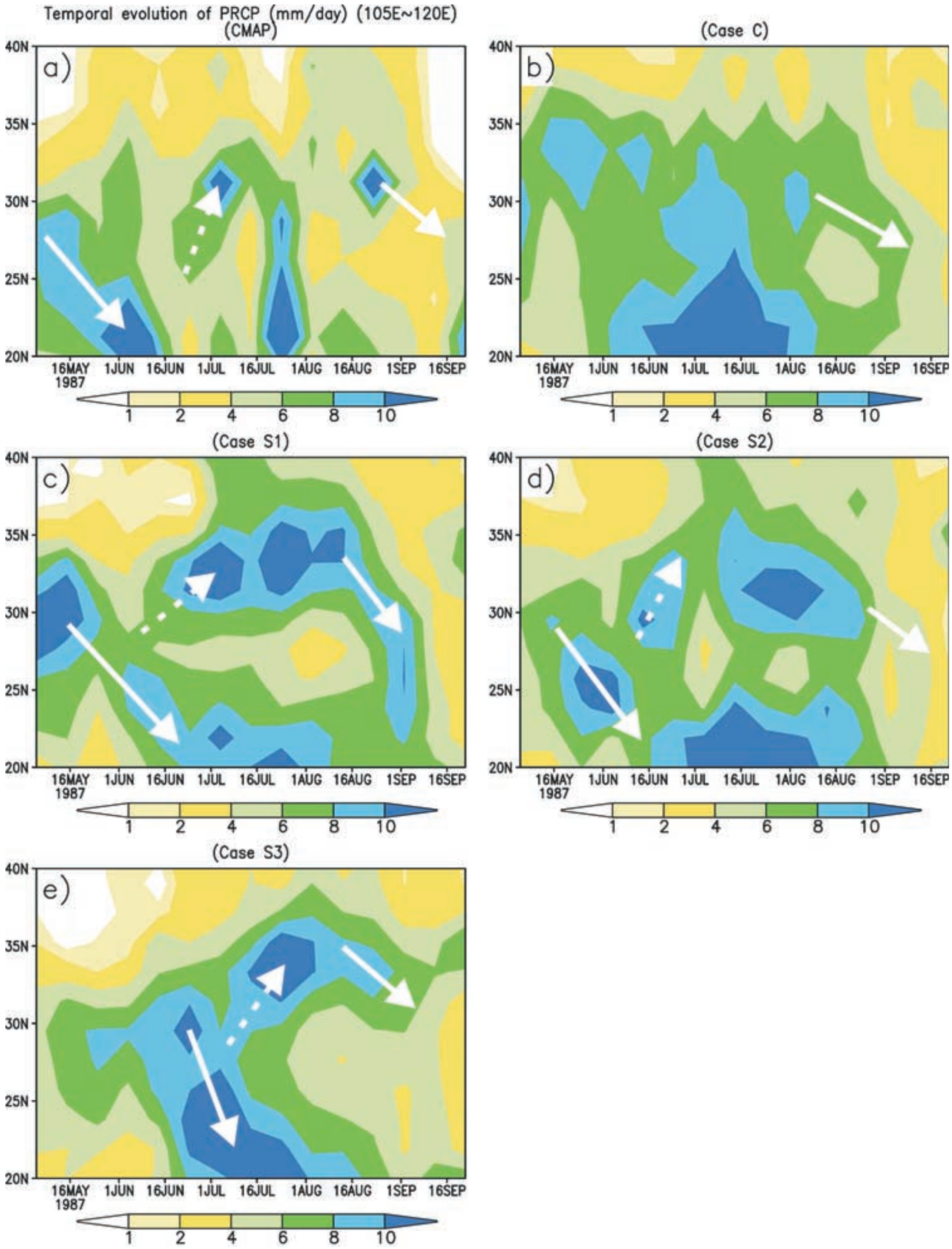

Figure 5. Temporal evolution of the 10-day mean precipitation (mm d^{-1}) averaged over 105°–120°E from May through September. (a) CMAP; (b) case C; (c) case S1; (d) case S2; (e) case S3.

band to the south and a divergence band to the north in east Asia (Figure 6b), however the southwesterly flow was unrealistically strong, pushing the convergence zone farther to the north. The cyclonic flow was too weak and the easterly wind between 30°N and 35°N almost disappeared. Case S1 produced circulation and associated convergences and divergences that were closer to the Reanalysis (Figure 6c). These differences in wind fields were consistent with those in precipitation (Figure 4). Each run in case C and case S1 gave very similar patterns.

[27] Many studies have investigated the mechanisms responsible for the atmospheric circulation. It has been found that the circulations in summer subtropics seem to be more related to thermal forcing, and the formation mechanism is more complicated compared with other latitudes [*Hoskins*, 1987]. In this study, it was found that circulations in May and June had the largest differences between two cases. To understand the causes, we analyzed the differences in surface heating. Table 2 shows the May average upward heating differences between case S1 and case C over the east Asian continent, and indicates the difference in sensible heat flux was dominant in the upward heating components. The May sensible heat flux, 850 hPa geopotential height, and the differences between cases C and S1 (Figure 7) showed that in case C, the east Asian area to the south of 30°N was a heat sink and the area to the north of 30°N was a source. In contrast, in case S1, the entire east Asian continent was a heat source. Therefore

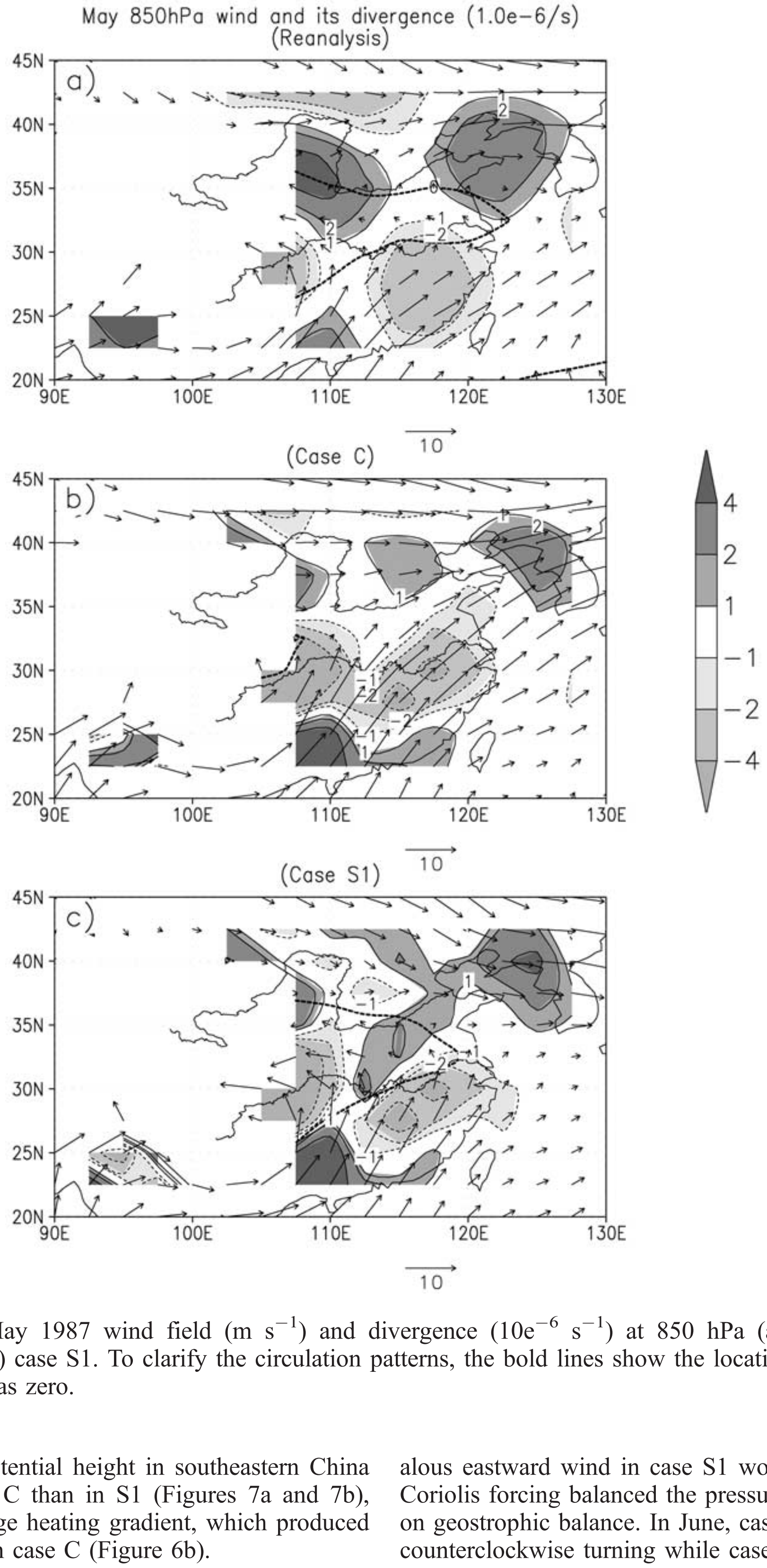

Figure 6. May 1987 wind field (m s^{-1}) and divergence (10e^{-6} s^{-1}) at 850 hPa (a) Reanalysis; (b) case C; (c) case S1. To clarify the circulation patterns, the bold lines show the locations where the zonal wind was zero.

the gradients of geopotential height in southeastern China were stronger in case C than in S1 (Figures 7a and 7b), consistent with the large heating gradient, which produced strong southwesterly in case C (Figure 6b).

[28] The counterclockwise turning of the low-level flow between 25°N and 32°N (Figure 6c) was consistent with the pressure gradient difference and the associated easterly wind anomaly between cases S1 and C in that region. Case S1 produced relative lower pressure to the south and relative higher pressure to the north (Figure 7c). An anomalous eastward wind in case S1 would be produced while Coriolis forcing balanced the pressure gradient force based on geostrophic balance. In June, case S1 still produced the counterclockwise turning while case C did not, because of the same cause as in May (not shown). In July and August, while the monsoon was mature, both cases S1 and C produced the turning. In another study [*Wu and Liu*, 2003] the July Reanalysis from 1980 to 1997 was used to analyze the relationship between circulation and boreal summer subtropical heating, which included vertical distri-

Table 2. Monthly Mean Surface Upward Heating Fluxes and Low-Level Air Temperature[a]

	Latent Heat Flux	Sensible Heat Flux	Short Wave Up	Long Wave Up	*T* (925 hPa)	*T* (850 hPa)
May, case S1 – case C	−15.9	26.9	−9	6.5	0.33	0.87
June, case S1 – case C	−9.4	35	−7.7	16.2	2.54	2.08

[a]Heating fluxes are given in W m^{-2}, and temperatures are given in °C (25°–35°N, 110°–120°E).

butions of long-wave radiative cooling, sensible heating and condensation heating in atmosphere. Condensation heating was identified as the main heating source in the east Asian lowland, which influenced the July monsoon. Our study reveals the role of vegetation processes, especially the spatial distribution of the surface heating in the processes, in the early stages of monsoon.

[29] Figure 8 shows the differences in JJA mean precipitation, vertically integrated moisture flux and its divergence, and evaporation between cases S1 and C. The

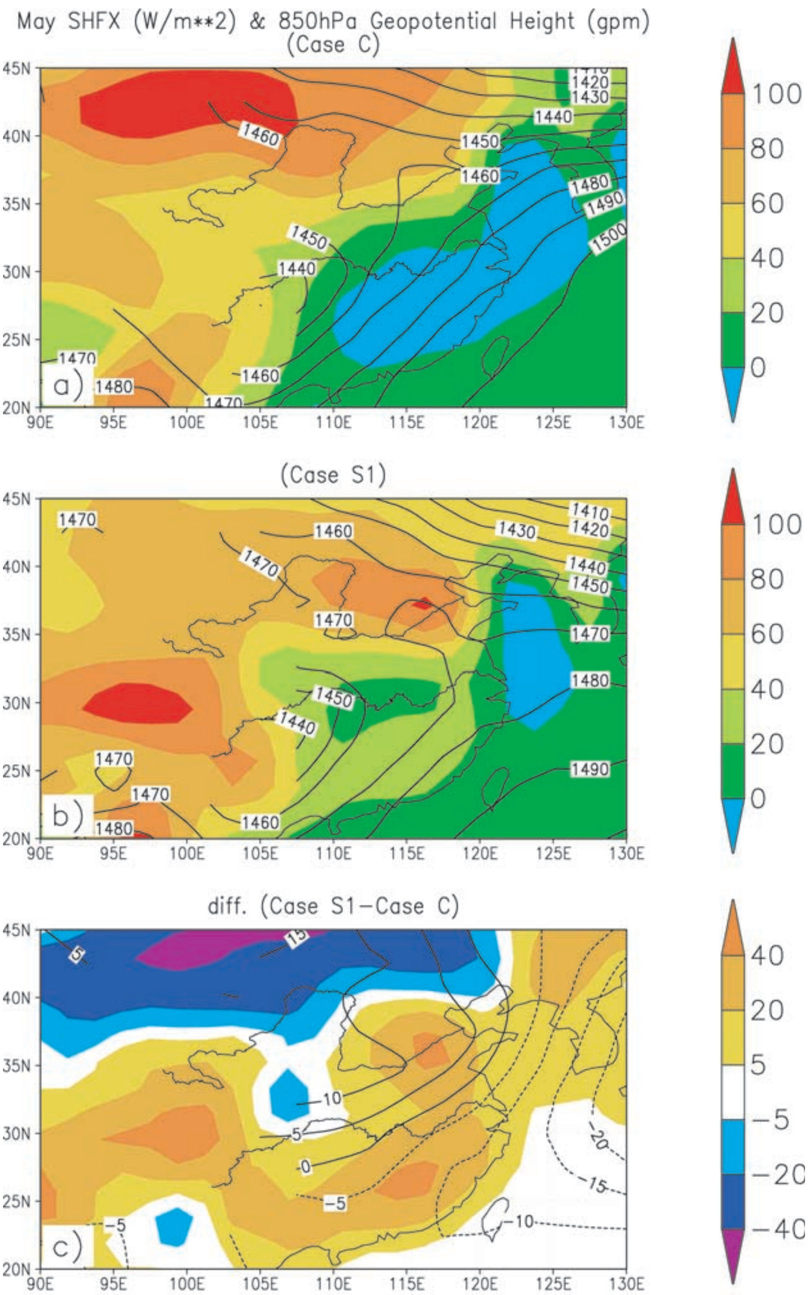

Figure 7. May sensible heat flux (W m^{-2}) and 850 hPa geopotential height (gpm). (a) Case C; (b) case S1; (c) case S1–case C.

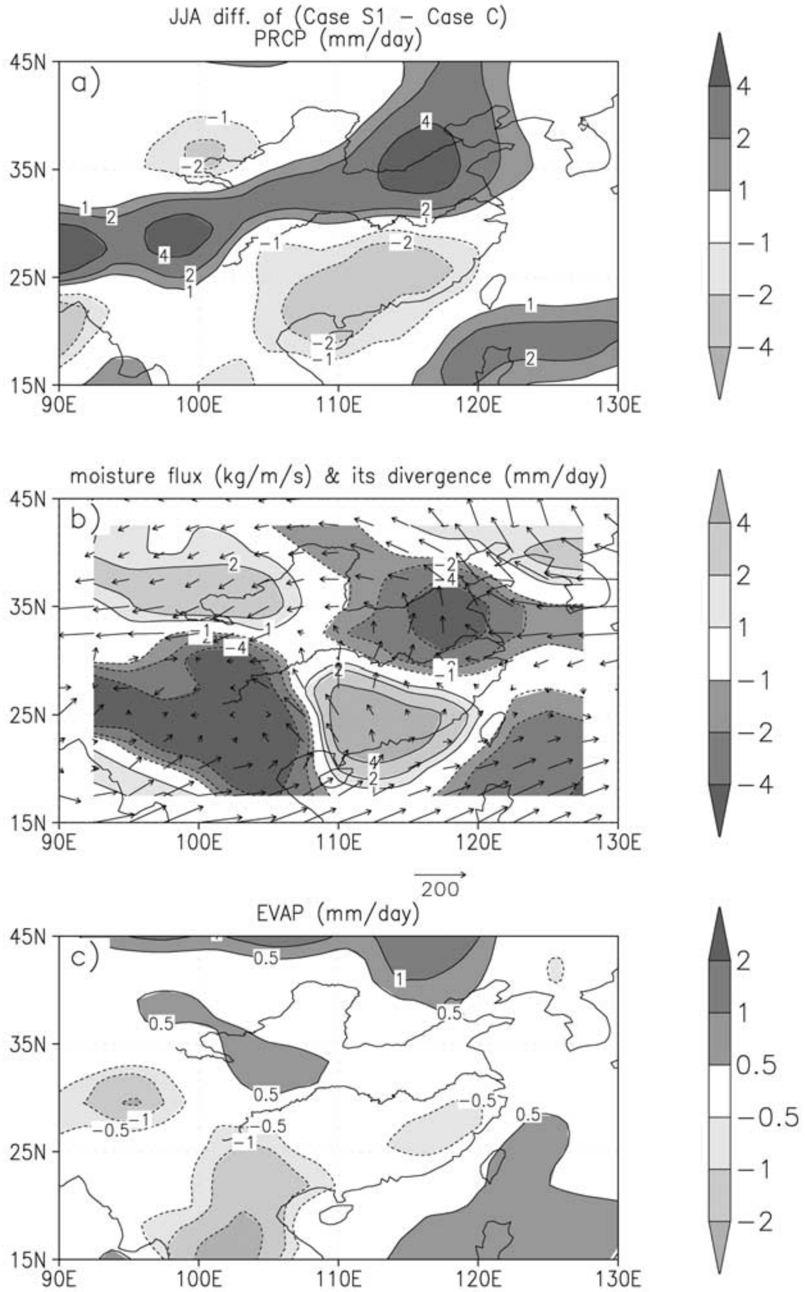

Figure 8. JJA mean differences between case S1 and case C (a) precipitation (mm d^{-1}); (b) Vertically integrated moisture flux (kg m^{-1} s^{-1}) and divergences (mm d^{-1}); (c) evaporation (mm d^{-1}).

northeast-southwest band with positive precipitation difference between 45°N and 25°N in Figure 8a was consistent with stronger moisture flux convergence (Figure 8b). The lower precipitation to the south of the Changjiang river and west of the Yellow river was located in the divergence areas (Figure 8b). Most changes in evaporation only appeared in the Indochina Peninsula and north of the Yellow River (Figure 8c). This indicates that the main differences in the monsoon precipitation simulation between cases C and S1 were related more closely to moisture-divergence field, the patterns of which were similar to the low-level wind field (not shown), rather than surface evaporation. Therefore it is necessary to examine the influence of land surface processes on the circulation to understand the evolution of the monsoon rainfall.

[30] The latitudinal and longitudinal means of several variables were evaluated to examine how land surface processes affected the northward jump. It was found that cases C and S1 had large differences in northward low-level moisture transport. Figure 9 shows the 10-day mean of 925 hPa specific humidity zonally averaged over 105°E and 120°E for cases C and S1. In early May, the northward transport of the moisture in case C was stronger and produced relatively wetter condition than case S1, as discussed in section 4.2.1 (Figure 4b). In the late part of June, the moist region in case S1 had a dramatic northward expansion

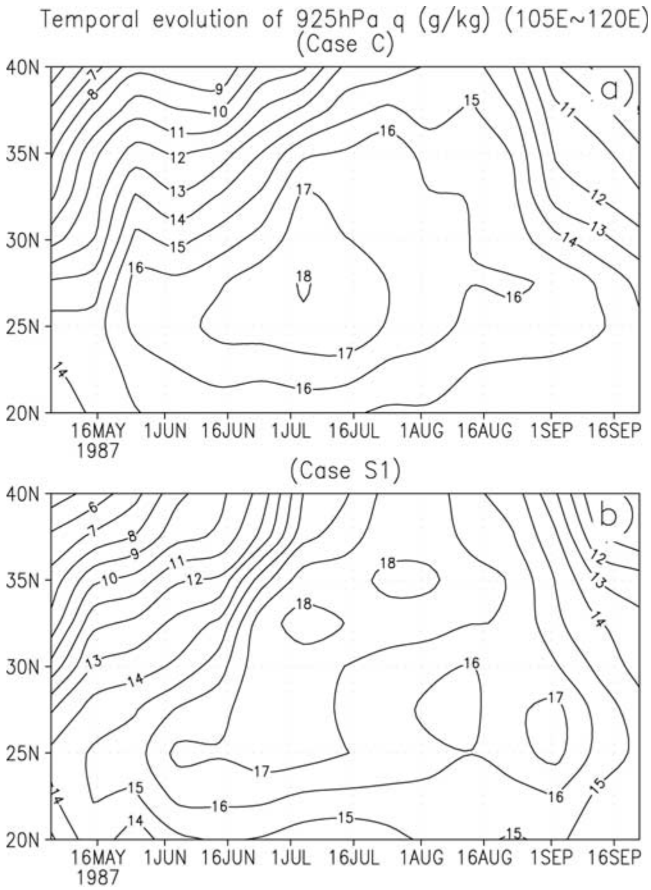

Figure 9. Temporal evolution of the 10-day mean specific humidity (g kg^{-1}) at 925 hPa averaged over 105°–120°E from May through September. (a) Case C; (b) case S1.

between 25°N and 40°N, which was consistent with the timing of the northward jump of the precipitation band (Figure 5c) and provided the necessary moisture. Case C, on the other hand, did not show such dramatic northward expansion. The maximum humidity (17 g kg^{-1} contour line) was confined to the south of the Changjiang river (at 30°N). Further analysis showed the differences in moisture fields were consistent with the differences in simulated meridional wind. The meridional wind at 925 hPa in case S1 also increased dramatically in the late part of June (Figure 10b), when the northward expansion of wet region occurred (Figure 9b). The 5 m s^{-1} contour line reached around 37°N. Case C, on the other hand, did not have an increase in meridional wind during June (Figure 10a). The 4 m s^{-1} contour line was confined to around 30°N. Since northward transport of the water vapor was the main moisture source of the east Asian summer monsoon (Figure 6), the differences shown in Figures 9 and 10 would have great impact on monsoon development. In the following, we further explore how land surface processes contribute to these differences.

[31] The abrupt northward jump in the east Asian monsoon is an important feature. Thus far there have only been theoretical studies of its cause, based on a quasi-geostrophic vorticity equation for a barotropic dissipative system with thermal forcing to investigate the mechanism of abrupt change of equilibria state [*Liu and Tao*, 1983; *Miao and Ding*, 1985; *Wang*, 1986]. These studies found that seasonally varying thermal forcing and interactions between thermal forcing and nonlinear motion of atmosphere under certain geographic conditions could produce abrupt changes in atmospheric circulation, but the abrupt change would not occur under weak meridional or zonal thermal gradients.

[32] Enlightened by these studies, we examined the surface heating sources to understand the role of land surface processes in the northward abrupt jump of rainfall band. The low-level temperature in case S1 in June was higher than in case C (Table 2), which would enhance the land-sea temperature gradient since the temperatures over the ocean were the same for the two cases (not shown). Table 2 shows the differences in radiative heating were not large, and case S1 had slightly less latent heat release from the surface. The major differences were in the sensible heat flux as in May. On the basis of the geostrophic balance in midlatitude, the northward wind (shown in Figure 10b) should be produced by the east-west pressure gradient. Among surface upward heating components, only sensible heat fluxes exhibited a clear east-west gradient.

[33] Figure 11 shows the 21–30 June mean sensible heat flux and geopotential height and the differences in 850 mbar. There was no clear gradient of sensible heat flux between the eastern part of the east Asian continent and the Pacific

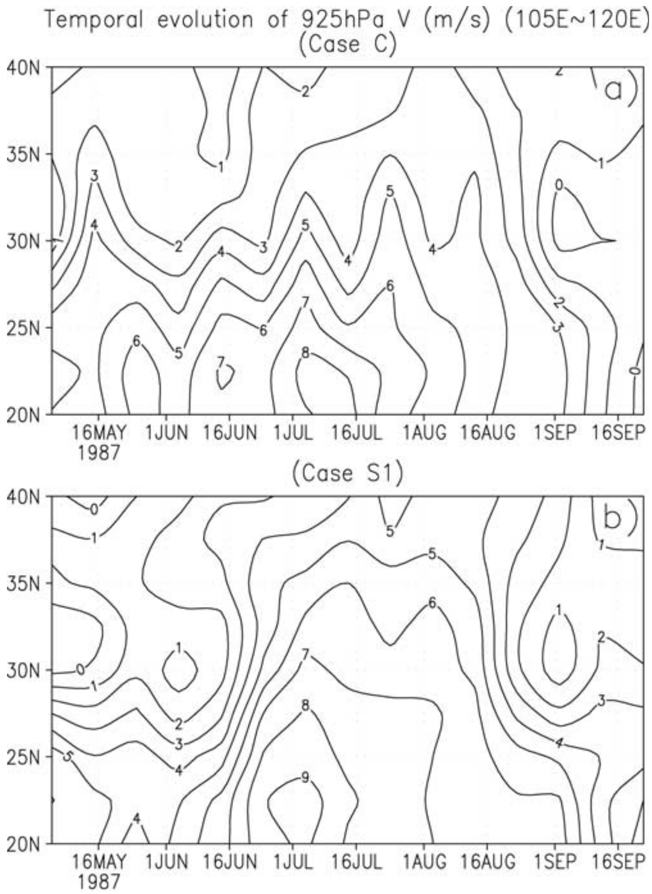

Figure 10. Temporal evolution of the 10-day mean meridional wind (m s^{-1}) at 925 hPa averaged over 105°–120°E from May through September. (a) Case C; (b) case S1.

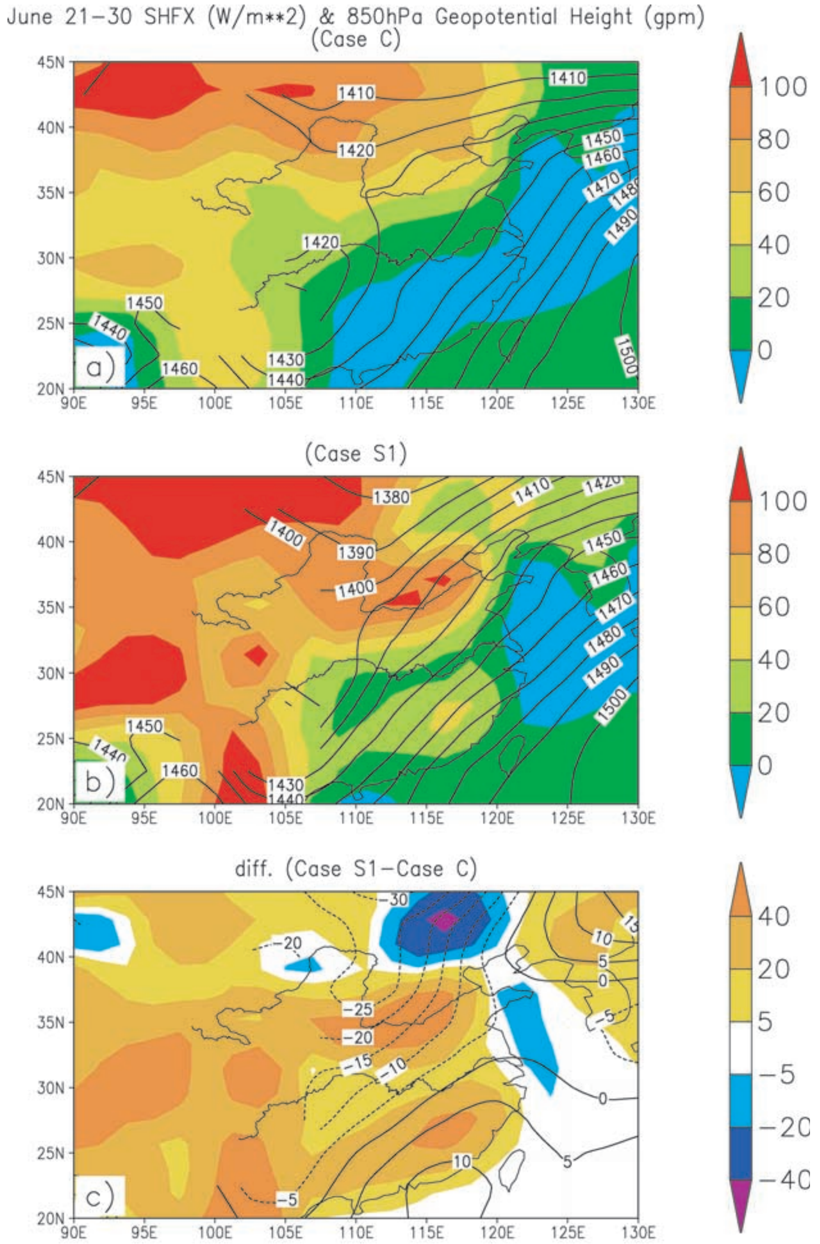

Figure 11. The 21–30 June sensible heat flux (W m^{-2}) and 850 hPa geopotential height (gpm). (a) Case C; (b) case S1; (c) case S1–case C.

Ocean in case C (Figure 11a). In fact, many parts of the land were heat sinks during June. In contrast to case C, S1 produced substantial east-west gradients of sensible heat flux between land and ocean, which in turn produced greater temperature gradients and consequent pressure gradients in the lower atmosphere (Figure 11b). The additional northward meridional wind was evident (Figure 11c). On the basis of these analyses and previous theoretical studies, we suggest that the greater east-west thermal gradient, which produced strong northward transport of moisture and a cyclone condition, may contribute to the abrupt northward jump of the monsoon.

4.3. West African Simulation

[34] The West African monsoon is relatively weak compared to the Asian monsoon [*Griffiths*, 1972; *Nicholson*, 1976]. The similarity of the climate in the east-west direction contrasts dramatically with the strong North-South gradient. The relationship between SST and seasonal to interannual rainfall variations in the Sahel region has long been discussed. Several observational and modeling studies have suggested that the Atlantic SST anomalies and global SST anomalies play important roles in producing rainfall anomalies over the Sahel and the adjoining regions [e.g., *Lamb*, 1978; *Hastenrath*, 1984; *Lamb and Peppler*, 1991; *Folland et al.*, 1991; *Palmer et al.*, 1992; *Rowell et al.*, 1995]. Meanwhile, the role of biophysical feedbacks in the Sahel region has also been examined [e.g., *Charney et al.*, 1977; *Walker and Rowntree*, 1977; *Sud and Fennessy*, 1982; *Laval and Picon*, 1986; *Kitoh et al.*, 1988; *Wang and Eltahir*, 1999]. These studies consistently demonstrated impacts of land surface conditions on the climate of the

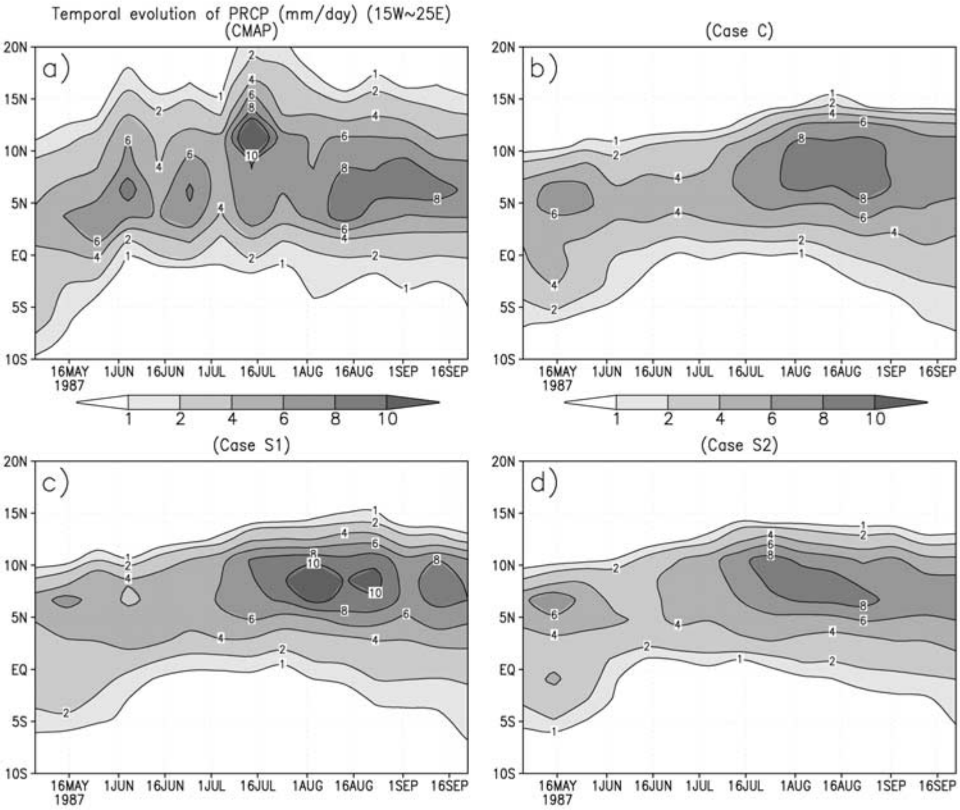

Figure 12. Temporal evolution of the 10-day mean precipitation (mm d^{-1}) averaged over 15°W to 25°E from May through September. (a) CMAP; (b) case C; (c) case S1; (d) case S2.

Sahel. Furthermore, biophysical models coupled with atmospheric models [e.g., *Xue and Shukla*, 1993; *Xue*, 1997; *Clark et al.*, 2001; *Wu et al.*, 2002; *Xue et al.*, 2003] have explored the role of land degradation in decadal Sahelian regional climate anomalies, including anomalous precipitation, higher surface temperature, lower river runoff, and the mechanisms responsible for the extended Sahel drought.

[35] In this section we present the results for the impact of two land surface parameterizations on the monsoon evolution and atmospheric circulation in northern Africa. Despite improvements in simulated total precipitation during the five-month simulation in case S1 (see Figure 3 for JJA mean) the processes of zonally mean monsoon evolution for the central and western Africa were not substantially different in cases C and S1 (Figure 12). In both the monsoon moved north in May and reached a maximum in August, but the intraseasonal variations were not well simulated. *Sultan and Janicot* [2000] identified a northward jump in the African monsoon from 5°N in May–June to 10°N in July–August (Figure 12a), which they attributed to African easterly waves and topographic effects. The models used here only produced a weak rainfall high in May, and showed no clear northward jump possibly because of limitation of the horizontal resolution. The May and June 1987 oscillation was a single year event, mainly because of internal variability (S. Janicot, LMD, personal communication, 2003), and was not simulated.

[36] Numerous studies have demonstrated the sensitivity of the Sahel regional climate to the land surface condition as mentioned above. Cases C and S1 had similar monthly mean albedo, surface roughness length, and initial soil moisture. Albedo and surface roughness are the two most important land parameters influencing the climate in the Sahel region [*Xue et al.*, 1997] and, unlike the midlatitudes, the interaction between one land parameter and atmosphere may be more important than multiple interactions [*Niyogi et al.*, 2002]. The similar monthly mean surface albedo and roughness lengths in cases C and S1 could explain why there was little difference in the simulated evolution of zonal mean precipitation in the Sahel. However, the differences in spatial distributions of simulated circulation as well as precipitation were still evident.

[37] The effects of land surface processes were manifested in wind fields and divergence. In the Reanalysis (Figure 13a), the southeasterly airflow from the Indian Ocean at 850 hPa became southwesterly after crossing the equator in central Africa, and formed a northeast-southwest convergence band between 10°E and 35°E, and between 20°S and the equator. The confluence of the southwesterly and northeasterly airflows formed another convergence zone over the Sahel, which was relevant to the summer monsoon in the region. Both cases C and S1 simulated the Sahel convergence zone well, although with different intensity (Figures 13b and 13c). Case C, however, failed to simulate a southwest-northeast convergence band from 10°E to 30°E because the turning of the southeasterly from the Indian Ocean was not as strong as in the Reanalysis (Figure 13a). In fact there was a stronger heating source along 10°N between 20°E and 40°E in case S1 (not shown). After crossing the equator, the heating induced airflow

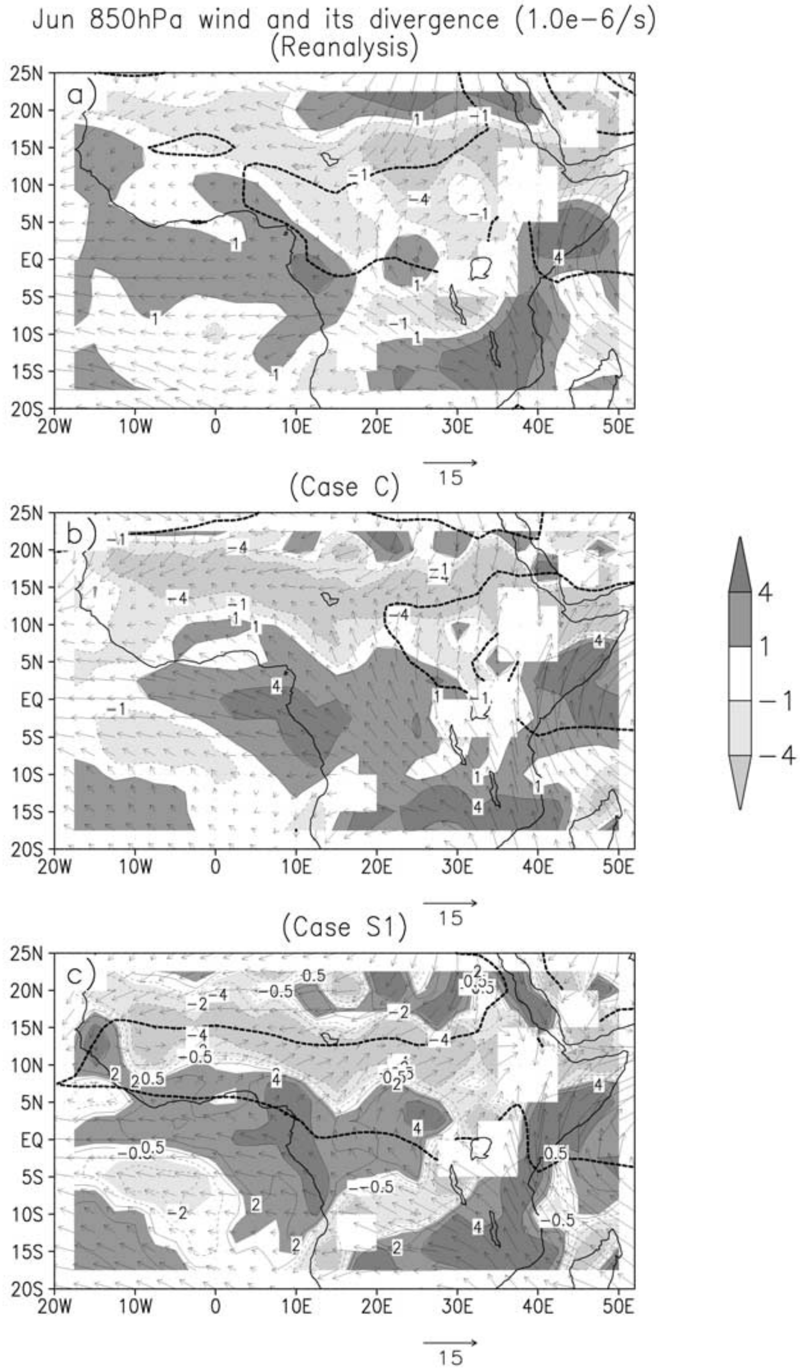

Figure 13. June 1987 wind field (m s^{-1}) and divergence ($10e^{-6}$ s^{-1}) at 850 hPa (a) Reanalysis; (b) case C; (c) case S1.

turned clockwise. This mechanism was consistent with the east Asian simulation (Figure 6). This heating source was missing in case C. The differences in wind fields also existed at 500 hPa. Convergence prevailed in central Africa in case C, which was opposite to that in the Reanalysis and case S1. The differences between case C and case S1 at 850 hPa and 500 hPa were also found in May and July.

[38] In addition to the circulation, cases C and S1 differed in rainfall intensity. In east Asia the differences in precipitation generally correlated with the changes in moisture flux (Figure 7) and it is interesting to examine the same relationship in Africa. We select the differences of these variables in June and August to exhibit the extremes (Figures 14 and 15). In June, although the evaporation reduction in East Africa and the coastal area of West Africa may have contributed to the precipitation decrease, the major rainfall change in the Sahel was consistent with the changes in moisture flux. Case S1 produced stronger moisture convergence and rainfall in the Sahel. A stronger moisture divergence in the coastal area and lower evaporation also contributed to the rainfall reduction (Figures 14a and 14b). In August the effect of evaporation prevailed

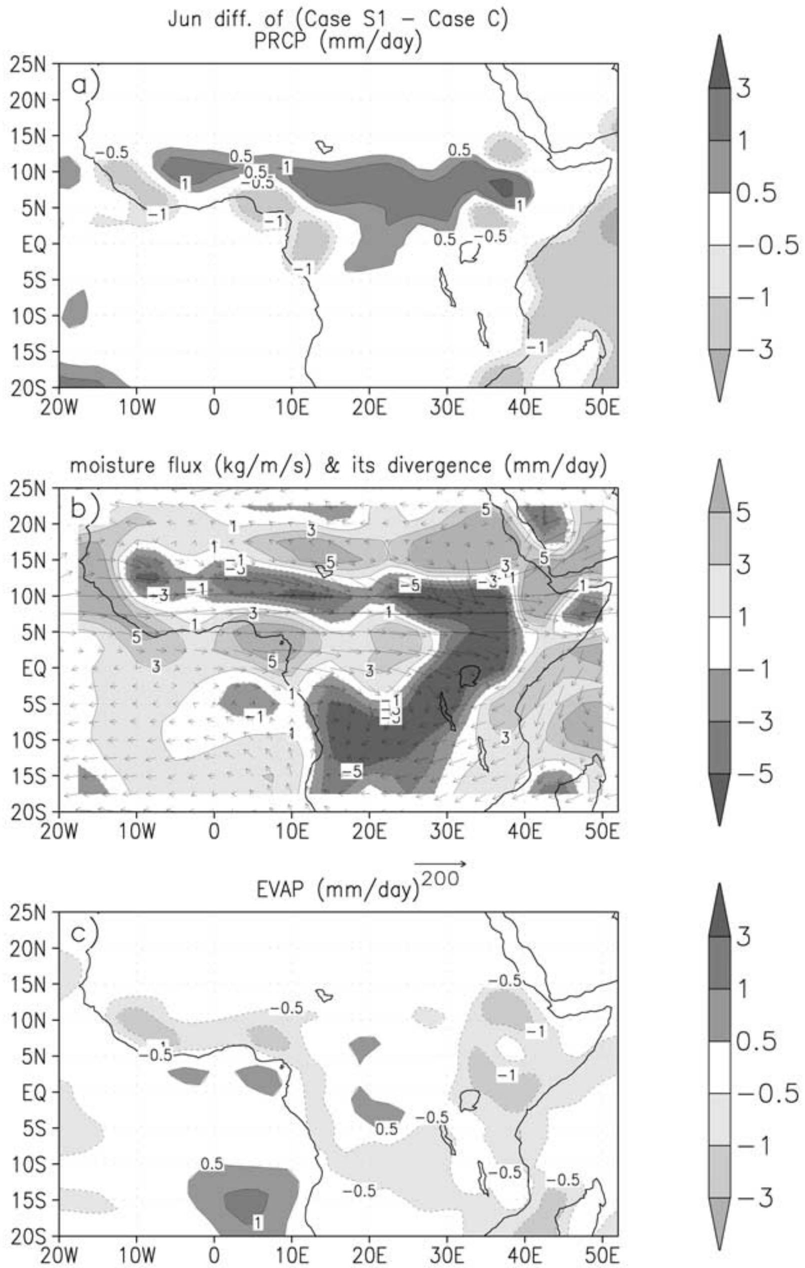

Figure 14. June differences between case S1 and case C (a) precipitation (mm d^{-1}); (b) vertically integrated moisture flux (kg m^{-1} s^{-1}) and divergences (mm d^{-1}); (c) evaporation (mm d^{-1}).

(Figure 15) and contributed to the large rainfall reduction in the Sahel, consistent with *Xue* [1997]. Compared with the east Asia, land surface evaporation played a more important role in the variation of West African monsoon. In addition to the Sahel region, the wind field and moisture convergences in case S1 and C also differed in central Africa (Figures 13c, 14b, and 15b), but there was not much precipitation in central Africa during the monsoon season and these differences did not affect the precipitation simulations there (Figures 14a and 15a).

5. Impact of Initial Soil Moisture

[39] Soil moisture is an important surface variable affecting the surface water and energy balances. Case S2 explored the effect of using the GSWP soil moisture as the initial condition for the NCEP GCM/SSiB (Figure 16). In general the soil in GSWP was drier than that in the Reanalysis except in West Africa, India and Bangladesh, East China, northwest South America, and southwest Australia (no GSWP data for Greenland and the Antarctic).

[40] It is clear that the JJA changes in precipitation and soil moisture were positively correlated, but the changes in soil moisture did not necessarily lead to changes in precipitation (Figure 17). Case S2 reduced the extra precipitation over the large continents and enhanced the Indian monsoon, but it was slightly dry in Africa (Figure 12d). *Dirmeyer* [2000] specified soil moisture during his entire model integration for 1987 and 1988, and found an improvement

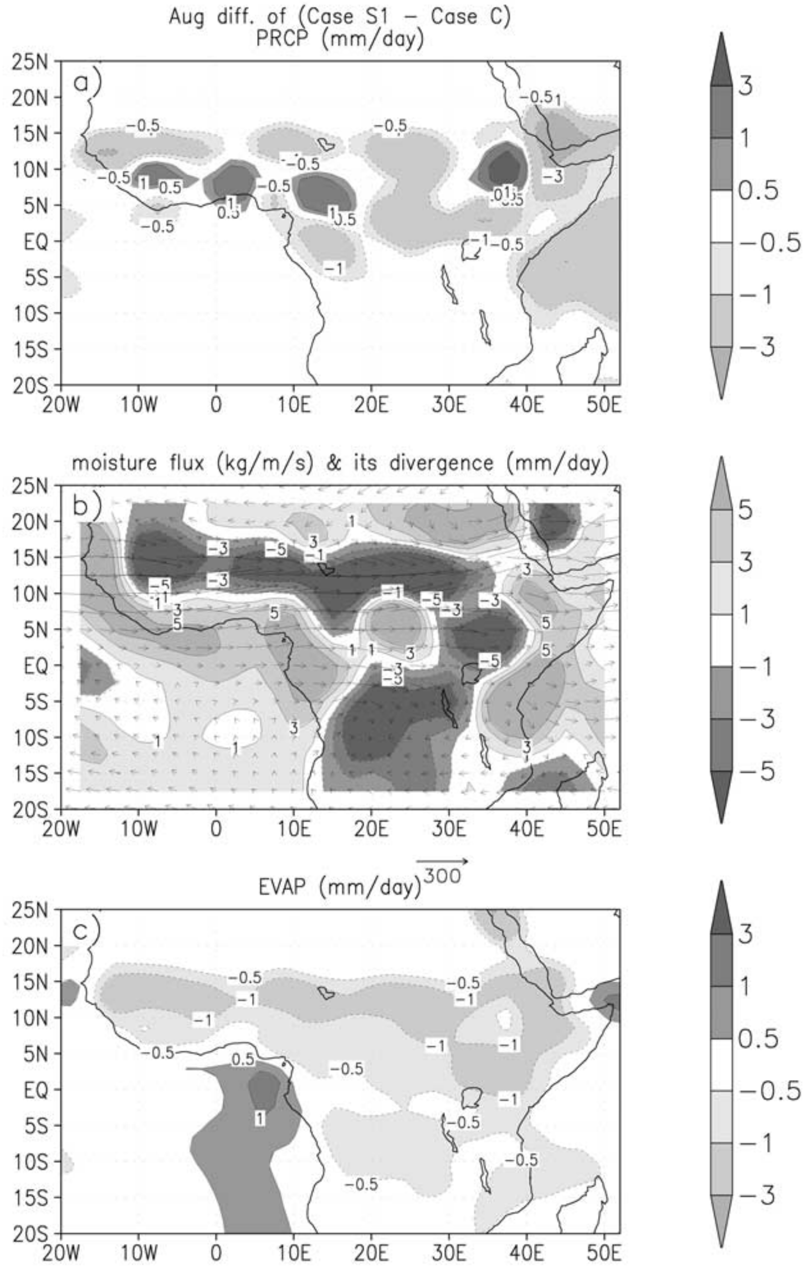

Figure 15. August differences between case S1 and case C (a) precipitation (mm d^{-1}); (b) vertically integrated moisture flux (kg m^{-1} s^{-1}) and divergences (mm d^{-1}); (c) evaporation (mm d^{-1}).

in the simulation of the pattern of precipitation globally and regionally, especially in monsoonal Asia.

[41] In this study the improvement in precipitation simulation in south Asia and east Asia was substantial. The year 1987 was an anomalously dry year over India. A counter-monsoon circulation anomaly at low level, associated with weaker Somali jet and Arabian Sea circulation, contributed to this summer drought [*Krishnamurti et al.*, 1989]. Cases C, S1, and S2 failed to catch the special features of the Indian monsoon for this year, but cases S1 and S2 still showed some improvements in monthly and seasonal means. For the Indian monsoon area (70°E to 85°E, 10°N to 25°N), the JJA precipitation was 6.2, 8.7 (±0.4), 6.7(±0.2), and 7.6(±0.8) mm d^{-1} for CMAP, cases C, S1, and S2, respectively. For the same area, but with land only, the JJA precipitation was 5.6, 6.7(±0.5), 4.6(±0.4), and 5.4(±0.8) mm d^{-1}, respectively. Case S1 produced the best simulation for the Indian monsoon as a whole. Case S2 had the best simulation for the Indian monsoon over land, but the standard deviations were large.

[42] The improvement in the east Asian simulation by case S2 was substantial, producing precipitation that was very similar to the May observation, with most heavy precipitation to the south of the Changjiang river and highest values near the coast of South China (Figure 4d). Case S2 also simulated the major features of the east Asian monsoon evolution processes (Figure 5d), with some differences in detail and intensity from case S1, providing further

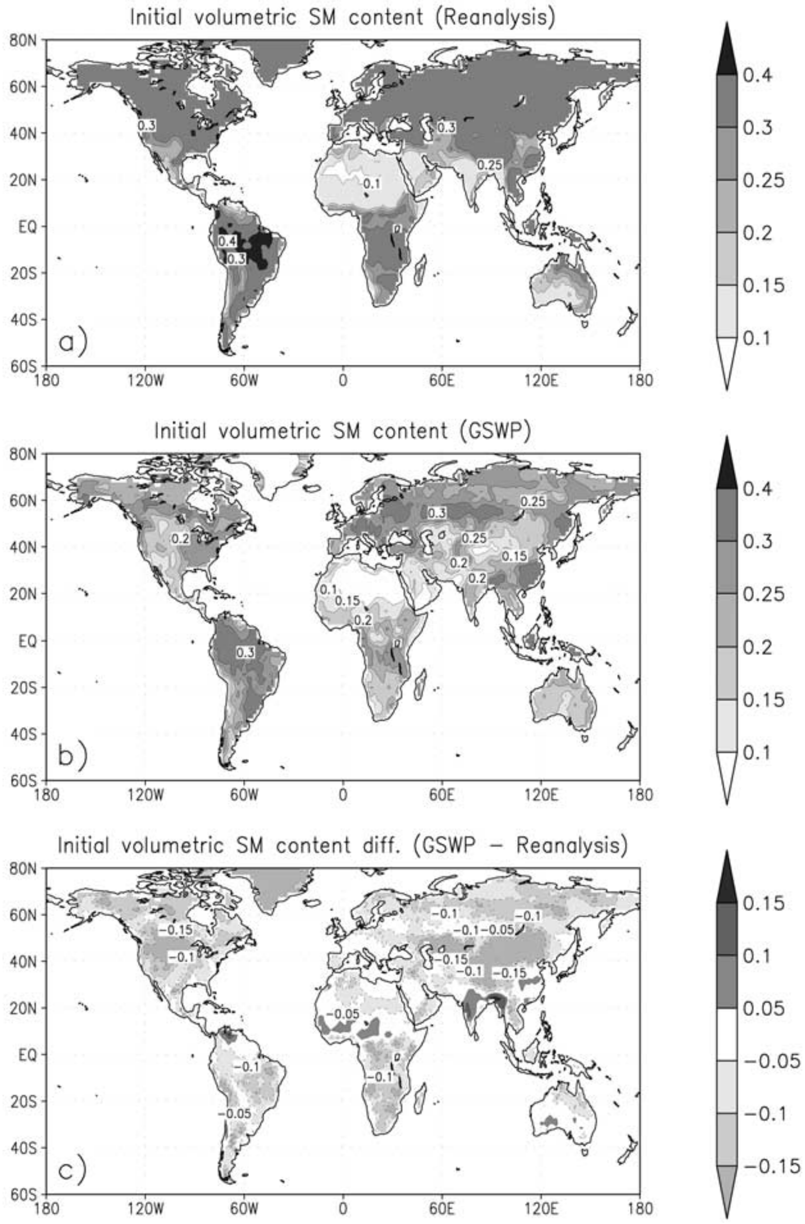

Figure 16. Initial volumetric soil water content for (a) Reanalysis; (b) GSWP; (c) GSWP−Reanalysis.

evidence that vegetation processes contribute to the northward jump of the monsoon. In fact, with the accurate initial soil moisture field, the simulated abrupt northward jump was closer to the observations (Figure 5d, dashed arrow), which suggests the soil moisture might influence the speed of the jump. A more detailed analysis revealed that most differences of precipitation between case S2 and S1were caused by the changes in convective precipitation.

6. Impact of the Land Cover Classification Map

[43] The impact of the specification of vegetation is illustrated by a comparison of case S3, using OLD SSiB MAP, and case S1, using NEW SSiB MAP. These produced different precipitation in tropical and subtropical regions (Figures 18a and 19a). Evaporation was the main cause of variations in precipitation on the Eurasian continent north of 40°N (Figure 18c). In the Inner Mongolian grassland and northeastern east Asia, the desert in case S3 produced less evaporation and precipitation. Divergence in northeastern east Asia was another factor that might have contributed to the reduction in precipitation (Figure 18b). On the other hand, in most parts of east Asia to the south of 40°N, the precipitation changes were associated with the dominant moisture flux convergence, consistent with the discussions in previous sections (Figure 8b). The desert in central Asia in case S3 produced a divergence region along 20°N and 30°N and a convergence region to the south. This was in general agreement with *Xue* [1996]. In east Asia the northward jump of the east Asian monsoon in case S3 was still evident (Figure 5e), but the timing was delayed by about

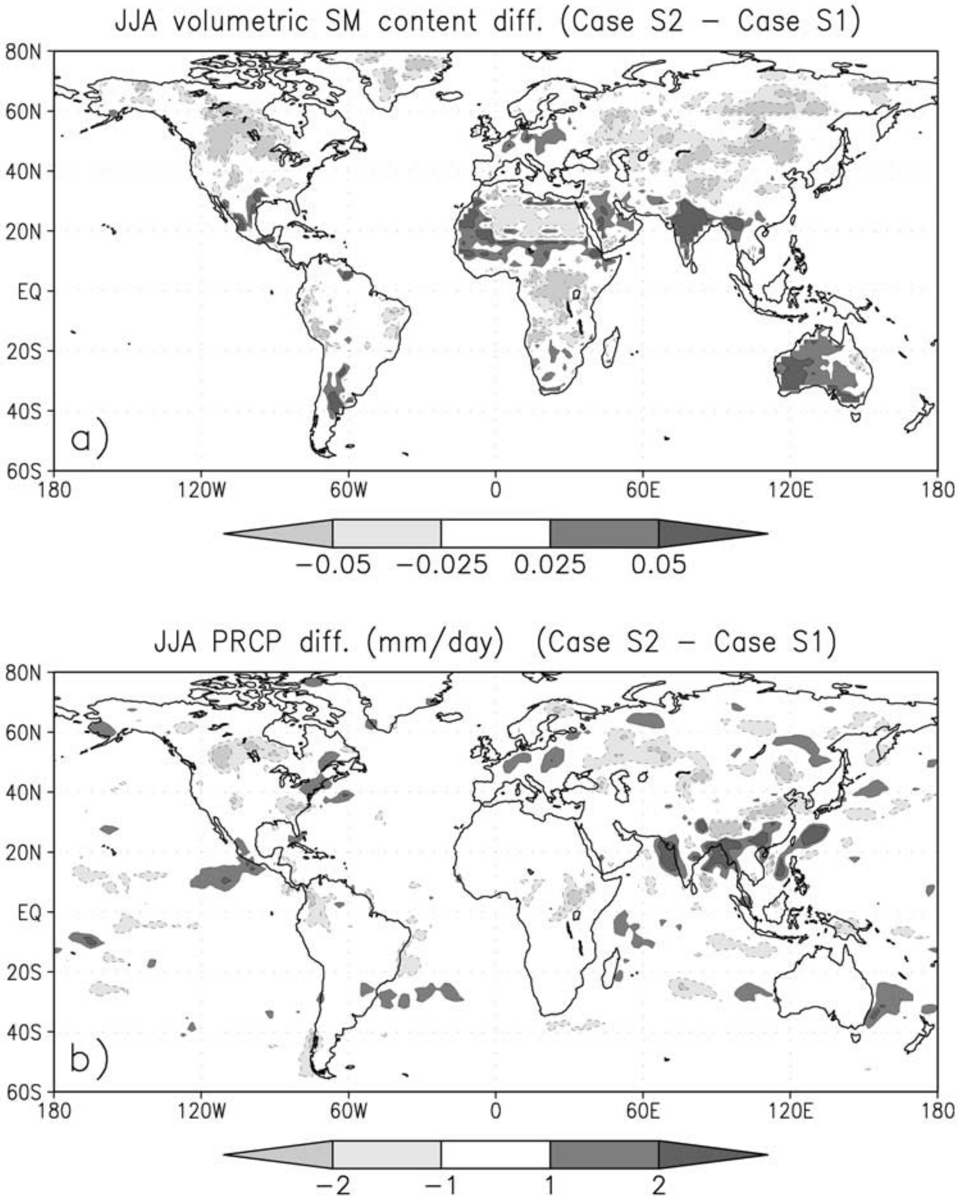

Figure 17. JJA differences between case S2 and case S1; (a) volumetric soil water content; (b) precipitation (mm d^{-1}).

one month, indicating that land cover change can modify the timing of the onset of the east Asian monsoon.

[44] In the Indian subcontinent there were no dramatic vegetation cover differences between NEW and OLD SSiB MAP. The precipitation differences between India and its surrounding ocean were mainly associated with changes in moisture fluxes, which was probably a response to land cover change in Eurasia to the north (Figures 18a and 18b). Although many studies have investigated the relationship between Eurasian snow cover and Indian monsoon, there have not been any studies investigating the relationship between Eurasian vegetation and Indian monsoon.

[45] The Sahara desert, where the vegetation classifications differed, had insufficient precipitation to exhibit any effect (Figure 19a) but there was an increase in induced divergence over a region between 10°N and 20°N and a convergence region to the south along the coastal area (Figure 19b): a dipole type of change noted by others [e.g., *Xue*, 1997]. The precipitation changes in case S3 in the African continent were coincident with these divergence and convergence regions. Since there was no substantial land cover change in central Africa, the reduction in evaporation (Figure 19c) was probably a response to the reduction in precipitation.

[46] NEW SSiB MAP improved the simulation of precipitation substantially in some important monsoon regions. For example, over northern Africa (10° to 40°E, and 0°N to 10°N), the JJA precipitations were 4.65, 4.41(±0.40), and 3.05(±0.35) mm d^{-1} for observation, case S1 and case S3, respectively. Even in southern China (between 110°E and 120°E and 25°N and 30°N), the error in simulation for JJA

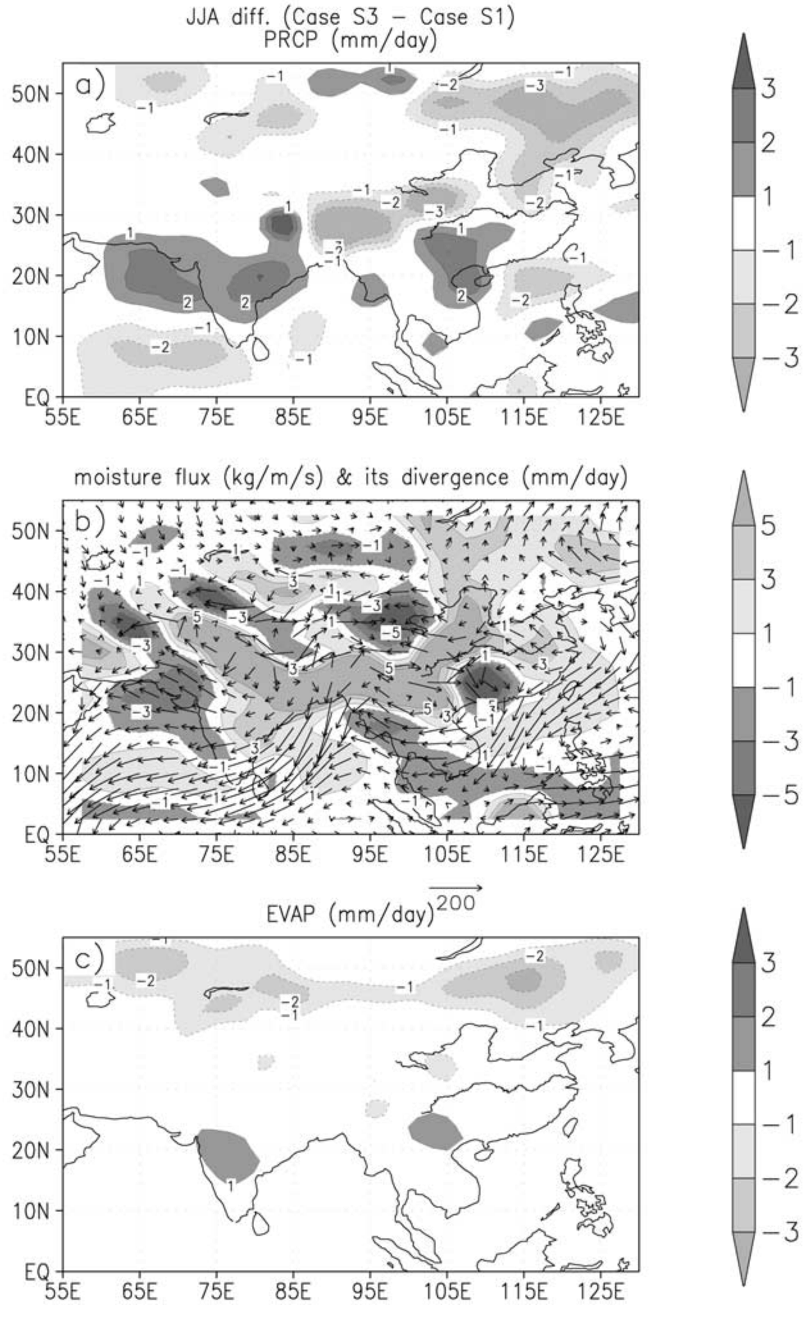

Figure 18. June differences between case S3 and case S1 in Asia (a) precipitation (mm d^{-1}); (b) vertically integrated moisture flux (kg m^{-1} s^{-1}) and its divergence (mm d^{-1}); (c) evaporation (mm d^{-1}).

precipitation was reduced from 1.17 mm d^{-1} in case S3 to 0.39 mm d^{-1} in case S1.

7. Discussion and Summary

[47] This study explores the impact of land surface processes on the structure and characteristics of the monsoon system with an emphasis on the evolution of precipitation. The results were obtained using the NCEP GCM coupled with two different land surface parameterizations that included or did not include vegetation processes. Because the study focused on intraseasonal variability with a temporal scale, in some cases, of only 5–10 days, three scenarios, differing in initial soil moistures and vegetation maps, with three initial conditions were used for each land surface parameterization to evaluate the robustness of the model results.

[48] In addition to the results for east Asia and West Africa, discussed above, we also examined the global mean precipitation and the precipitation over the land (Table 3). The standard deviations were substantially smaller than the differences between case C and case Ss and were of the same order of magnitude for each month. Case C simulated the global climate with reasonable accuracy. Cases S1 and S3 provided small, but consistent improvements for each month in the simulations, which indicated that the improve-

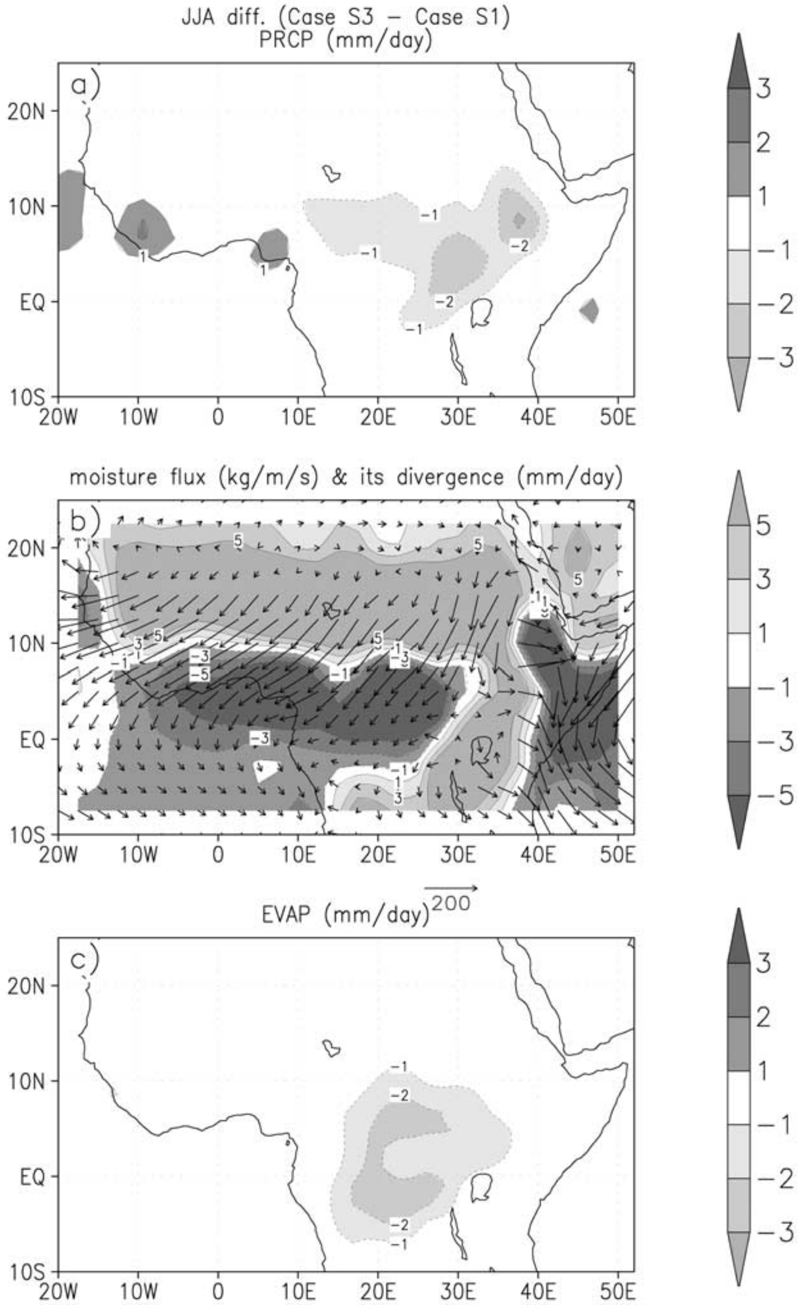

Figure 19. June differences between case S3 and case S1 in Africa (a) precipitation (mm d^{-1}); (b) vertically integrated moisture flux (kg m^{-1} s^{-1}) and its divergence (mm d^{-1}); (c) evaporation (mm d^{-1}).

ments at a regional scale were not at the cost of global realism. It was interesting to note that case S3 had the best simulation of the global mean (Table 3). This was mainly because, after classifying most of east Asia as desert, the wet bias in the model simulation was substantially reduced. For the area between 105°E and 125°E and 30°N and 50°N, the observed, case S1 and case S3 JJA precipitation was 3.73, 5.89(±035), and 4.08(±0.33) mm d^{-1}, respectively. Therefore the underlying cause of the "better" global mean precipitation in case S3 was most likely due to weakness in the GCM and/or land surface model or problems in vegetation parameter specification. There are no direct measurements of the vegetation and soil parameters for most parts of the world.

[49] Although the simulations by using the two parameterizations were compared with each other and with observations, the aim of this study was principally to understand better the influence of biophysical processes on the processes of monsoon development. The results show that at the planetary scale, two different land surface parameterizations produced similar monthly mean simulations of precipitation (Figure 3). The differences in global means were small (Table 3). However, at the continental and synoptic scales, more complete represen-

Table 3. Mean Precipitation Over Land and Over the Globe[a]

	May	June	July	August	JJA	s.d. JJA
Xie and Arkin [1997]	1.84 (2.74)	2.10 (2.75)	2.16 (2.81)	2.23 (2.77)	2.04 (2.77)	
Case C	2.41 (2.98)	2.36 (3.07)	2.62 (3.04)	2.58 (2.99)	2.52 (3.03)	0.04 (0.01)
Case S1	2.13 (2.89)	2.30 (3.02)	2.56 (3.00)	2.45 (2.90)	2.43 (2.97)	0.04 (0.01)
Case S2	1.87 (2.88)	2.16 (2.95)	2.46 (2.97)	2.34 (2.89)	2.32 (2.94)	0.02 (0.01)
Case S3	1.73 (2.82)	2.01 (2.96)	2.27 (2.90)	2.31 (2.85)	2.20 (2.90)	0.06 (0.005)

[a]Mean precipitation over the globe is given in parenthesis. Values are in mm d^{-1}. Here, s.d., standard deviation.

tation of land surface processes improved the simulation of the structure and characteristics of the monsoon systems.

[50] Cases S1 and C used the similar monthly mean albedo as well as surface roughness length, and the same initial soil moisture. However, the two land surface schemes produced different surface water and energy balances, different partitioning of latent heat and sensible heat fluxes (the Bowen ratio), and different latitudinal and longitudinal thermal gradients at the surface. The effects were mainly manifested in the temporal evolution of the monsoon, its strength, the spatial distribution of precipitation, and associated circulation at continental and synoptic scales. Under the three scenarios, the GCM with a biosphere model consistently simulated the abrupt northward movement of the east Asian monsoon unlike the GCM/SOIL model runs.

[51] Furthermore, this study shows the surface processes influenced the turning of the low-level wind counterclockwise or clockwise during the premonsoon or early monsoon stages, the low-level land/sea temperature gradient, wind flow, and moisture transport, which were related to the monsoon development. This study shows that under unstable conditions, not only the low-frequency mean forcings from the land surface, but also the perturbation processes of vegetation forcing described in SSiB on much shorter timescales, such as radiative flux/canopy interaction and transpiration, may be crucial in the evolution of the monsoon. Since 1987 alone was simulated for this study, further investigations under different scenarios (such as different SSTs) will be necessary to confirm this finding.

[52] In previous studies, we found that specifications of land degradation in Sahel and east Asia allowed climate simulations to reproduce decadal anomaly patterns of precipitation and surface temperature [*Xue and Shukla*, 1993; *Xue*, 1996, 1997]. Furthermore, better representations of land surface processes in a regional model improved the short-term (24 and 48 hours) simulations of extreme climate events, such as the 1993 U.S. flood [*Xue et al.*, 2001]. The results from this study show that land surface processes may also be important for intraseasonal simulations. However, the land/atmosphere interactions are complex and nonlinear as shown in Figure 3 and the dominant mechanisms depend on temporal and spatial scales and background climate conditions.

[53] Our findings show that better specification of the initial soil moisture improved seasonal simulation, mainly in the intensity of the simulated variables. It also suggests possible relationships between vegetation distribution in the Eurasian continent and the Indian monsoon intensity, as well as land degradation in east Asia and timing of the east Asian monsoon onset, indicating the importance of accurate land cover maps.

[54] Both the NCEP soil submodel and SSiB are physically based models, which was evident by the fact that no empirical tuning was needed in this study when the soil model was replaced with SSiB, and the differences between the simulations by the two models could be clearly related to physical and dynamic processes, even in the complexity of a GCM. These conclusions, however, need to be evaluated using different models. Although this version of the NCEP GCM produced substantially better east Asian simulations than, for example, by *Xue* [1996], substantial biases were still evident (e.g., Figure 3). The accurate simulation and prediction of monsoons, especially the Asian monsoon, is a formidable task and some crucial improvements remain to be made, such as the simulation of precipitation in south Asia. This study showed that high-quality observational data of land cover and assimilated soil moisture help identify the role of land surface parameterizations in monsoon simulation and, more generally, in land/atmosphere interactions.

[55] **Acknowledgments.** The authors thank Masao Kanamitsu, UCSD, for providing the NCEP GCM code and for his support; Song-You Hong and Hua-Lu Pan, NCEP, for help in this work; Eugenia Kalnay, University of Maryland, for her support; C. Roberto Mechoso of UCLA Xiuji Zhou of the Chinese Academy of Meteorological Sciences (CAMS), and Serge Janict of the Laboratoire de Meteorologie Dynamique, France, for discussions; Pingping Xie of NCEP for meteorological data; and Paul Dirmeyer of COLA for GSWP data. Michio Yanai of UCLA, Guoxiong Wu of the Institute of Atmospheric Physics, Chinese Academy of Sciences, Longxun Chen and Weiliang Li of CAMS, Akiyo Yatagai of the Research Institute of Humanity and Nature, Japan, and K.-M. Lau of NASA have provided comments for this manuscript. Funding was provided by NSF grants EAR 9706403 and ATM-0097260 and NASA grants NAG5-9014 and NAG5-9329. The model runs were carried out on the NCAR and NCEP supercomputers.

References

Barnett, T. P., L. Dumenil, U. Schlese, E. Roeckner, and M. Latif (1989), The effect of Eurasian snow cover on regional and global climate variations, *J. Atmos. Sci.*, *46*, 661–685.

Businger, J. A., J. C. Wyngaard, Y. Izumi, and E. G. Bradley (1971), Flux-profile relationships in the atmospheric surface layer, *J. Atmos. Sci.*, *28*, 181–189.

Charney, J. G., W. K. Quirk, S.-H. Chow, and J. Kornfield (1977), A comparative study of the effects of albedo change on drought in semi-arid regions, *J. Atmos. Sci.*, *34*, 1366–1385.

Chen, L., Q. Shu, and H. Lu (1991), *East Asian Monsoon* (in Chinese), 362 pp., China Meteorol. Press, Beijing.

Chen, L., W. Li, and P. Zhao (2001), On the process of summer monsoon onset over east Asia, *Acta Meteorol. Sin.*, *15*, 436–449.

Clark, D. B., Y. Xue, R. Harding, and P. J. Valdes (2001), Modeling the impact of land surface degradation on the climate of tropical North Africa, *J. Clim.*, *14*, 1809–1822.

Deardorff, J. W. (1977), Efficient prediction of a ground surface temperature and moisture with inclusion of a layer of vegetation, *J. Geophys. Res.*, *83*, 1889–1903.

Dey, B., and O. S. R. U. Bhanu Kumar (1982), An apparent relationship between Eurasian snow cover and the advanced period of the Indian summer monsoon, *J. Appl. Meteorol.*, *21*, 1929–1932.
Ding, Y. (1994), *Monsoon in China*, 419 pp., Kluwer Acad., Norwell, Mass.
Dirmeyer, P. A. (2000), Using a global soil wetness dataset to improve seasonal climate simulation, *J. Clim.*, *13*, 2900–2922.
Dirmeyer, P. A., A. J. Dolman, and N. Sato (1999), The pilot phase of the Global Soil Wetness Project, *Bull. Am. Meteorol. Soc.*, *80*, 851–878.
Dorman, J. L., and P. Sellers (1989), A global climatology of albedo, roughness length and stomatal resistance for atmospheric general circulation models as represented by the Simple Biosphere Model (SiB), *J. Appl. Meteorol.*, *28*, 833–855.
Douville, H., and J.-F. Royer (1996), Sensitivity of the Asian summer monsoon to an anomalous Eurasian snow cover within the Météo-France GCM, *Clim. Dyn.*, *12*, 449–466.
Douville, H., F. Chauvin, and H. Broqua (2001), Influence of soil moisture on the Asian and African monsoons. Part I: Mean monsoon and daily precipitation, *J. Clim.*, *14*, 2381–2403.
Flohn, H. (1957), Large-scale aspects of the "summer monsoon" in South and east Asia, *J. Meteorol. Soc. Jpn.*, *75*, 180–186.
Folland, C. K., J. Owen, M. N. Ward, and A. Colman (1991), Prediction of seasonal rainfall in the Sahel region using empirical and dynamical methods, *J. Forecast.*, *1*, 21–56.
Grell, G. A., J. Dudhia, and D. R. Stauffer (1994), A description of the fifth generation Penn State/NCAR Mesoscale Model (MM5), *NCAR Tech. Note NCAR/TN-398+STR*, 121 pp., Natl. Cent. for Atmos. Res., Boulder, Colo.
Griffiths, J. F. (1972), General climatology, in *Climates of Africa*, edited by J. F. Griffiths, pp. 1–35, Elsevier Sci., New York.
Hahn, D. J., and J. Shukla (1976), An apparent relationship between Eurasian snow cover and Indian monsoon rainfall, *J. Atmos. Sci.*, *33*, 2461–2462.
Hansen, M. C., R. S. DeFries, J. R. G. Townshend, and R. Sohlberg (2000), Global land cover classification at 1 km spatial resolution using a classification tree approach, *Int. J. Remote Sens.*, *21*, 1303–1330.
Hastenrath, S. (1984), International variability and annual cycle: Mechanisms of circulation and climate in the tropical Atlantic sector, *Mon. Weather Rev.*, *112*, 1097–1107.
Hoskins, B. J. (1987), Diagnosis of forced and free variability in the atmosphere, in *Atmospheric and Oceanic Variability*, edited by H. Cattle, pp. 57–73, James Glaisher House, Bracknell, UK.
Kalnay, E., M. Kanamitsu, and W. E. Baker (1990), Global numerical weather prediction at the National Meteorological Center, *Bull. Am. Meteorol. Soc.*, *71*, 1410–1428.
Kalnay, E., et al. (1996), The NMC/NCAR 40-year Reanalysis Project, *Bull. Am. Meteorol. Soc.*, *77*, 437–471.
Kanamitsu, M., J. C. Alpert, K. A. Campana, P. M. Caplan, D. G. Deaven, M. Iredell, B. Katz, H.-L. Pan, J. Sela, and G. H. White (1991), Recent changes implemented into the global forecast system at NMC, *Weather Forecast.*, *6*, 425–435.
Kistler, E., et al. (1999), The NCEP/NCAR 50-year Reanalysis, *Bull. Am. Meteorol. Soc.*, *82*, 247–268.
Kitoh, A., K. Yamazaki, and T. Tokioka (1988), Influence of soil moisture and surface albedo changes over the African tropical rain forest on summer climate investigated with the MRI-GCM-I, *J. Meteorol. Soc. Jpn.*, *66*, 65–85.
Krishnamurti, T. N., H. S. Bedi, and M. Subramaniam (1989), The summer monsoon of 1987, *J. Clim.*, *2*, 321–340.
Kuchler, A. W. (1983), World map of natural vegetation, in *Goode's World Atlas*, 16th ed., pp. 16–17, Rand McNally, New York.
Lamb, P. J. (1978), Large-scale tropical Atlantic surface circulation patterns associated with sub-Saharan weather anomalies, *Tellus*, *30*, 240–251.
Lamb, P. J., and R. A. Peppler (1991), West Africa, in *Teleconnections Linking Worldwide Climate Anomalies*, edited by M. Glantz, R. W. Katz, and N. Nicholls, pp. 121–189, Cambridge Univ. Press, New York.
Lau, K.-M., and W. Bua (1998), Mechanisms of monsoon-Southern Oscillation coupling: Insights from GCM experiments, *Clim. Dyn.*, *14*, 759–779.
Lau, K.-M., G. J. Yang, and S. H. Shen (1988), Seasonal and intraseasonal climatology of summer monsoon rainfall over east Asia, *Mon. Weather Rev.*, *116*, 18–37.
Laval, K., and L. Picon (1986), Effect of a change of the surface albedo of the Sahel on climate, *J. Atmos. Sci.*, *43*, 2418–2429.
Liu, C., and S. Tao (1983), Northward jumping of subtropical highs and CUSP catastrophe, *Sci. Sin., Ser. B, Engl. Ed.*, *26*, 1065–1074.
Liu, X., and M. Yanai (2002), Influence of Eurasian spring snow cover on Asian summer rainfall, *Int. J. Climatol.*, *22*(9), 1075–1089.
Louis, J.-F. (1979), A parametric model of vertical eddy fluxes in the atmosphere, *Boundary Layer Meteorol.*, *17*, 187–202.
Matthews, E. (1984), Prescription of land-surface boundary conditions in GISS GCM II: A simple method based on high-resolution vegetation data bases, *NASA Tech. Memo., NASA TM-86096*, 20 pp.
Matthews, E. (1985), Atlas of archived vegetation, land-use and seasonal albedo data sets, *NASA Tech. Memo., NASA TM-86199*, 53 pp.
Meehl, G. A. (1994), Influence of the land surface in the Asian summer monsoon: External conditions versus internal feedbacks, *J. Clim.*, *7*, 1033–1049.
Miao, J., and M. Ding (1985), Catastrophe theory of seasonal variation, *Sci. Sin., Ser. B, Engl. Ed.*, *28*, 1079–1092.
Miyakoda, K., and J. Sirutis (1986), Manual of the E-physics, Geophys. Fluid Dyn. Lab., Princeton Univ., Princeton, N. J.
Nicholson, S. E. (1976), A climatic chronology for Africa: Synthesis of geological, historical, and meteorological information and data, Ph.D. thesis, Univ. of Wisc., Madison.
Niyogi, D. S., Y. Xue, and S. Raman (2002), Hydrological feedback in land-atmosphere coupling: Comparison of a tropical and a midlatitudinal regime, *J. Hydrometeorol.*, *3*, 39–56.
Palmer, T. N., C. Brankovic, P. Viterbo, and M. J. Miller (1992), Modeling interannual variations of summer monsoons, *J. Clim.*, *5*, 399–417.
Pan, H.-L., and L. Mahrt (1987), Interaction between soil hydrology and boundary layer developments, *Boundary Layer Meteorol.*, *38*, 185–202.
Paulson, C. A. (1970), Mathematical representation of wind speed and temperature profiles in the unstable atmospheric surface layer, *J. Appl. Meteorol.*, *9*, 857–861.
Robock, A., M. Mu, K. Vinnikov, and D. Robinson (2003), Land surface conditions over Eurasia and Indian summer monsoon rainfall, *J. Geophys. Res.*, *108*(D4), 4131, doi:10.1029/2002JD002286.
Rowell, D. P., C. K. Folland, K. Maskell, and M. N. Ward (1995), Variability of summer rainfall over tropical North Africa (1906–92): Observation and modeling, *Q. J. R. Meteorol. Soc.*, *121*, 669–704.
Shi, L., and E. A. Smith (1992), Surface forcing of the infrared cooling profile over the Tibetan Plateau. Part II: Cooling-rate variation over large-scale Plateau domain during summer monsoon transition, *J. Atmos. Sci.*, *49*, 823–844.
Sud, Y. C., and M. Fennessy (1982), A study of the influence of surface albedo on July circulation in semi-arid regions using the GLAS GCM, *J. Clim.*, *2*, 105–125.
Sultan, B., and S. Janicot (2000), Abrupt shift of the ITCZ over West Africa and intra-seasonal variability, *Geophys. Res. Lett.*, *27*, 3353–3356.
Vernekar, A. D., J. Zhou, and J. Shukla (1995), The effect of Eurasian snow cover on the Indian monsoon, *J. Clim.*, *8*, 248–266.
Walker, J., and P. R. Rowntree (1977), The effect of soil moisture on circulation and rainfall in a tropical model, *Q. J. R. Meteorol. Soc.*, *103*, 29–46.
Wang, G. (1986), Some factors determining the jump of the sub-tropical highs (in Chinese), *Sci. Meteorol. Sin.*, *1*, 50–60.
Wang, G., and E. A. B. Eltahir (1999), Biosphere-atmosphere interactions over West Africa. I: Development and validation of a coupled dynamic model, *Q. J. R. Meteorol. Soc.*, *126*, 1239–1260.
Webster, P. J. (1987), The elementary monsoons, in *Monsoons*, edited by J. F. Fein and P. L. Stephens, pp. 3–32, John Wiley, New York.
Webster, P. J., V. Magana, T. N. Palmer, J. Shukla, R. A. Tomas, M. Yanai, and T. Yasunari (1998), Monsoons: Processes, predictability, and the prospects for prediction, *J. Geophys. Res.*, *103*(C7), 14,451–14,510.
Weng, H. Y., K. M. Lau, and Y. K. Xue (1999), Long term variations of summer rainfall over China and its possible link to global sea-surface temperature variability, *J. Meteorol. Soc. Jpn.*, *4*, 845–857.
Willmott, C. J., and K. Klink (1986), A representation of the terrestrial biosphere for use in global climate studies, in *ISLSCP: Proceedings of an International Conference Held in Rome, Italy, 2–6 December 1985*, pp. 109–112, Eur. Space Agency, Paris.
Wu, G., and Y. M. Liu (2003), Summertime quadruplet heating pattern in the subtropics and the associated atmospheric circulation, *Geophys. Res. Lett.*, *30*, 1201–1204.
Wu, G., L. Sun, Y. Liu, H. Liu, S. Sun, and W. Li (2002), Impacts of land surface processes on summer climate, in *Selected Papaers of the Fourth Conference on East Asia and Western Pacific Meteorology and Climate*, edited by C. P. Chang et al., pp. 64–76, World Sci., River Edge, N. J.
Xie, P., and P. A. Arkin (1997), Global precipitation: A 17-year monthly analysis based on gauge observations, satellite estimates and numerical model outputs, *Bull. Am. Meteorol. Soc.*, *78*, 2539–2558.
Xue, Y. (1996), The impact of desertification in the Mongolian and the Inner Mongolian Grassland on the regional climate, *J. Clim.*, *9*, 2173–2189.
Xue, Y. (1997), Biosphere feedback on regional climate in tropical North Africa, *Q. J. R. Meteorol. Soc.*, *123*, 1483–1515.
Xue, Y., and J. Shukla (1993), The influence of land surface properties on Sahel climate. Part I: Desertification, *J. Clim.*, *6*, 2232–2245.

Xue, Y., P. J. Sellers, J. L. Kinter III, and J. Shukla (1991), A simplified biosphere model for global climate studies, *J. Clim.*, *4*, 345–364.
Xue, Y., H. G. Bastable, P. A. Dirmeyer, and P. J. Sellers (1996a), Sensitivity of simulated surface fluxes to changes in land surface parameterization: A study using ABRACOS data, *J. Appl. Meteorol.*, *35*, 386–400.
Xue, Y., M. J. Fennessy, and P. J. Sellers (1996b), Impact of vegetation properties on U.S. summer weather prediction, *J. Geophys. Res.*, *101*(D3), 7419–7430.
Xue, Y., J. Elbers, F. J. Zeng, and A. J. Dolman (1997), GCM parameterization for Sahelian land surface processes, in *HAPEX-Sahel West Central Supersite: Methods, Measurements and Selected Results*, *Rep. 130.HM/07.97*, edited by P. Kabat, S. Prince, and L. Prihodko, pp. 289–297, Winand Staring Cent. for Integrated Land, Soil and Water Res., Wageningen, Netherlands.
Xue, Y., F. J. Zeng, K. Mitchell, Z. Janjic, and E. Rogers (2001), The impact of land surface processes on the simulation of the U.S. hydrological cycle: A case study of 1993 US flood using the Eta/SSiB regional model, *Mon. Weather Rev.*, *129*, 2833–2860.
Xue, Y., R. W. A. Hutjes, R. J. Harding, M. Claussen, S. Prince, E. F. Lambin, S. J. Alan, and P. Dirmeyer (2003), The Sahelian climate, in *Vegetation, Water, Humans, and the Climate*, edited by P. Kabat et al., chap. 5, pp. 57–76, Springer-Verlag, New York.
Yanai, M., and T. Tomita (1998), Seasonal and interannual variability of atmospheric heat sources and moisture sinks as determined from NCEP/NCAR reanalysis, *J. Clim.*, *11*, 463–482.
Yang, S., and K.-M. Lau (1998), Influences of sea surface temperature and ground wetness on Asian summer monsoon, *J. Clim.*, *11*, 3230–3246.
Yasunari, T., A. Kitoh, and T. Tokioka (1991), Local and remote responses to excessive snow mass over Eurasia appearing in the northern spring and summer climate: A study with the MRI GCM, *J. Meteorol. Soc. Jpn.*, *62*, 473–487.
Yatagai, A., and T. Yasunari (1994), Trends and decadal-scale fluctuations of surface air temperature and precipitation over China and Mongolia during the recent 40 year period (1951–1990), *J. Meteorol. Soc. Jpn.*, *72*, 937–957.
Yatagai, A., and T. Yasunari (1995), Interannual variations of summer precipitation in the arid/semi-arid regions in China and Mongolia: Their regionality and relation to the Asian summer monsoon, *J. Meteorol. Soc. Jpn.*, *73*, 909–923.

R. DeFries and S. Prince, Department of Geography, University of Maryland, College Park, Le Frak Hall, College Park, MD 20742, USA. (rd63@umail.umd.edu; sp43@umail.umd.edu)

Y. Jiao, Department of Earth and Atmospheric Sciences, University of Quebec at Montreal, 550 Sherbrooke West Road, Montreal, Canada H3A 1B9. (jiao@atlas.sca.uqam.ca)

H.-M. H. Juang, NCEP/NWS/NOAA, WWBG Room 204, 5200 Auth Road, Camp Springs, MD 20746, USA. (wd20hh@ncep.noaa.gov)

W.-P. Li, R. Vasic, and Y. Xue, Department of Geography, University of California, Los Angeles, 1255 Bunche Hall, UCLA Box 951524, Los Angeles, CA 90095-1524, USA. (wli@weber.sscnet.ucla.edu; rvasic@weber.sscnet.ucla.edu; yxue@geog.ucla.edu)